IEEE Access
Multidisciplinary | Rapid Review | Open Access Journal

SPECIAL SECTION ON ADVANCES ON HIGH PERFORMANCE WIRELESS NETWORKS FOR AUTOMATION AND IIOT

Received 23 December 2022, accepted 7 March 2023, date of publication 13 March 2023, date of current version 17 March 2023.

Digital Object Identifier 10.1109/ACCESS.2023.3256888

RESEARCH ARTICLE

M-Ary Aggregate Spread Pulse Modulation With Pulse-Shaping Power Control for Highly Scalable LPWANs

ALEXEI V. NIKITIN[1], (Member, IEEE), AND RUSLAN L. DAVIDCHACK[2]
[1]Nonlinear LLC, Wamego, KS 66457, USA
[2]School of Computing and Mathematical Sciences, University of Leicester, LE1 7RH Leicester, U.K.

Corresponding author: Alexei V. Nikitin (avn@nonlineacorp.com)

This work was supported in part by Pizzi Inc., Denton, TX, USA.

ABSTRACT M-ary Aggregate Spread Pulse Modulation (M-ASPM) is the physical layer (PHY) modulation technique that is well suited for use in low-power wide-area networks (LPWANs). Notably, M-ASPM combines high energy-per-bit efficiency, robustness, resistance to interference, and a number of other favorable technical characteristics, with the spread-spectrum ability to maintain the capacity of an uplink-focused network while extending its range. However, when all M-ASPM nodes transmit with the same average power, implementation of such capacity-preserving range extension may become impractical in complicated propagation environments with greatly varying path losses. Favorably, the efficiency of M-ASPM with constant-envelope pulses can be maintained effectively the same as the efficiency of transmitting a continuous constant-envelope waveform. Then the transmit power of different nodes can be adjusted, without sacrificing the transmission efficiency, to compensate for differences in the path attenuation. This enables us to significantly simplify planning and management of the network. In addition, such a variable-power approach generally increases the network capacity and the average energy efficiency of the nodes, as compared with the arrangement of the nodes with a constant transmit power. In this paper, we outline a practical approach to implementing such an energy-efficient M-ASPM power control, that can be used for scaling LPWANs with realistic desired and/or actual areal distributions of the uplink nodes under diverse propagation conditions.

INDEX TERMS Aggregate spread pulse modulation (ASPM), the Internet of things (IoT), LoRa, low-power wide-area network (LPWAN), M-ary ASPM (M-ASPM), physical layer (PHY), spread spectrum, time-bandwidth product (TBP).

I. INTRODUCTION AND MOTIVATION

The M-ary Aggregate Spread Pulse Modulation (M-ASPM) is a physical layer (PHY) modulation scheme that combines high energy-per-bit efficiency, and a number of other appealing technical aspects, with the ability to maintain the network capacity while extending its range. It is a recently introduced modulation technique, and many of its promising features have not yet been explored and/or quantified. Its first description was given in [1], where the main goal was to examine the spectral and energy efficiencies of coherent and noncoherent M-ASPM variants, and evaluate the bit error probability for M-ASPM links in an additive white Gaussian noise (AWGN) channel. Then in [2] the primary focus was on quantifying M-ASPM networks' scalability, that is, on the spread-spectrum properties of M-ASPM. In both [1] and [2] we also discuss in passing such M-ASPM link properties as their resistance to multipath delay and Doppler spreads, and to impulsive noise commonly present in industrial environments.

In [2], we show that when M-ASPM is used as a spread-spectrum technique (that is, when it operates at the spectral efficiencies below the maximum for a given M, where $\log_2 M$ is the number of bits encoded in a single pulse), its processing gain is proportional to the M-ASPM's average interpulse interval (IpI). As a result, this interval directly affects such link properties as its time-on-air (ToA),

The associate editor coordinating the review of this manuscript and approving it for publication was Lei Shu.

the signal-to-interference ratio (SIR) margin and, for a given transmit power, the link's range. In particular, both the ToA and the SIR margin are effectively proportional to the IpI, while the range, if it is a monotonically increasing function of the path loss, is a monotonically increasing function of the IpI. This enables us to maintain the M-ASPM network's capacity while extending its range. Importantly, we demonstrate that such capacity-preserving range extension can be achieved for numerous desired and/or actual areal distributions of the uplink nodes.

But before addressing placement of the nodes at arbitrary locations over a wide area, let us first revisit the simple case when all nodes with equal transmit power are placed at a given distance from the receiver (e.g., in the same physical location), and adopt a number of simplifying idealizations. Among those are the assumptions of the "data equality" of the nodes (so that each node has the same data payload per unit time), the same frequency band and the value of M for all nodes, and a random access protocol. If we assume that the path loss is a function of the distance only, then the nodes can be placed along a circle centered at the receiver. We can also quantify the constraint on the co-PSF collisions by α, $0 < \alpha \leq 1$, where α is the product of the number of the same-PSF nodes and the duty cycle of their transmissions. Note that the case $\alpha = 1$ would correspond to a continuous transmission in a given PSF channel. For a random access protocol, the value of α that maximizes the throughput would be smaller than unity. For example, for the pure ALOHA [3] the maximum throughput would be achieved for $\alpha = 1/2$.

If the path loss is a function of the range only, then the total number of end nodes that can be placed at the distance d from the receiver can be expressed as

$$C(d) = m(d)\, C_1(d), \tag{1}$$

where $C_1(d)$ is the number of nodes for a single PSF channel (subject to the constrains on the co-PSF collisions) and $m(d)$ is the number of PSF channels that can be used without causing unacceptable deterioration in the bit error rate (BER).

For an uplink node in a given PSF channel, the transmissions from the nodes in all other $(m-1)$ channels produce interference that will generally increase the BER. For the increase in the uncoded BER to remain below a certain level, the reciprocal of the average SIR for this interference should not exceed the respective "SIR margin" $\Delta_{\rm SIR}$. This constraint can be expressed as

$$\mathrm{SIR}^{-1} = (m-1)\,\alpha \leq \Delta_{\rm SIR}. \tag{2}$$

When an M-ASPM node transmits at the spectral efficiencies below the maximum for a given M (that is, in the spread-spectrum region), both its SIR margin and its range increase with the IpI. Thus the SIR margin is an increasing function of the range, and the value of $m(d)$ in (1) can be obtained as

$$m(d) = 1 + \frac{\Delta_{\rm SIR}(d)}{\alpha}. \tag{3}$$

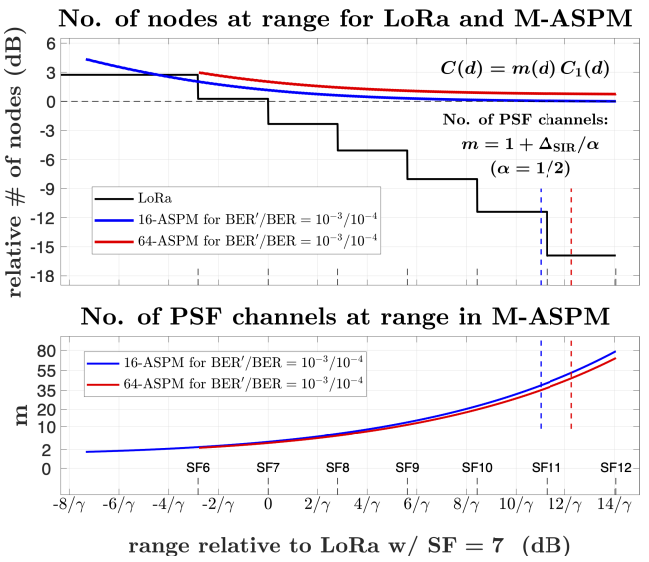

FIGURE 1. Number of uplink end nodes that can be placed at given range in M-ASPM and LoRa, and number of M-ASPM PSF channels that can be used at this range. AWGN channel, noncoherent detection, random access protocol, and power-law path loss model with path-loss exponent γ are assumed. In LoRa, SF = 6 through SF = 12 are used, and inter-SF collisions are ignored. In M-ASPM, number m of employed PSF channels varies according to SIR margins $\Delta_{\rm SIR}(r)$ for BER′/BER = $10^{-3}/10^{-4}$. Vertical dashed lines (blue for 16-ASPM and red for 64-ASPM) indicate ranges below which M-ASPM's ToA per payload remains smaller than that for LoRa with SF = 12.

For convenience, let us allow the number of the PSF channels $m(d)$ resulting from (3) to take non-integer values. We can then assume that $\lfloor m \rfloor$ channels are "fully" utilized (i.e., operating at the co-PSF constraint α), and one channel is only "partially" utilized, so that the product of the number of nodes in this channel and their duty cycle is below α.

Let us also assume that the payload overhead (e.g., for the header and synchronization) uses the same number of pulses for each payload. Then, for a constant-size data payload, the transmission ToA is proportional to the IpI, and the number of nodes per channel is inversely proportional to the IpI. Further, if the SIR margin is defined as in [2] (also in Section II-C of this paper), $\Delta_{\rm SIR}$ is proportional to the IpI. This leads to

$$C(d) = \left(1 + \frac{\Delta_{\rm SIR}(d)}{\alpha}\right) C_1(d) = C_1(d) + C_{\rm lim}, \tag{4}$$

where $C_{\rm lim} = \Delta_{\rm SIR}(d)\, C_1(d)/\alpha$, and to

$$C(d \to \infty) = C_{\rm lim} = const. \tag{5}$$

Thus, if there is no constraint on the maximum ToA of a payload, extending the range beyond a sufficiently large d can be performed without a significant decrease in the total capacity (the number of nodes). This is quantitatively illustrated in Fig. 1, for a power-law path loss with the path-loss exponent γ [4].

The physical ranges and the capacities in Fig. 1 are shown in reference to LoRa (short for "Long Range"), a popular modulation technique for low-power wide-area networks (LPWANs) [5], [6]. For a given number of bits per waveform,

LoRa has the same energy-per-bit efficiency as M-ASPM. (In LoRa, this number is represented by the ''spreading factor'' (SF), which can typically take values from 6 to 12.) Thus, when operating under effectively the same physical conditions (e.g., the same physical frequency band, transmit power, antenna gains, and various system attenuations such as insertion, path, and matching losses, etc.), LoRa represents a suitable benchmark for M-ASPM.

To obtain the numerical results presented in Fig. 1, the same constraint ($\alpha = 1/2$) is used for the co-SF (in LoRa) and co-PSF (in M-ASPM) collisions, and we neglect the increase in the payload overhead in LoRa for larger SFs. The maximum LoRa ranges for each SF are for the uncoded AWGN BER $= 10^{-4}$, and in the calculation of the total LoRa capacities the interference among the channels is completely ignored. For M-ASPM, the SIR margins are calculated for the increase in the uncoded bit error rates in an AWGN channel from BER $= 10^{-4}$ to BER$' = 10^{-3}$.

As can be seen in the upper panel of Fig. 1, the number of M-ASPM nodes that can be placed at the range for LoRa with SF $= 12$ is only about 20% smaller than the number of nodes at the range for SF $= 7$. This is in contrast with LoRa, for which such a range extension leads to a more than an order of magnitude (approximately 40 times) reduction in the number of nodes. As a result, for example, for ranges beyond that of LoRa with SF $= 11$, 16-ASPM offers about 40 times more nodes than LoRa, and for 64-ASPM this difference increases to almost 50-fold.

Without a constraint on the maximum ToA of a payload, the M-ASPM range can be extended far beyond that of LoRa, even for relatively small values of M. However, a maximum allowed ToA (and thus a minimal data rate) for a given frequency band can impose a practical limitation on the M-ASPM range. For example, for noncoherent detection the maximum spectral efficiency of M-ASPM is the same as LoRa's with SF $= \log_2 M$. Then, if the minimal allowed data rate is equal to that of LoRa with a given SF, the effective range of M-ASPM with $\log_2 M <$ SF will be smaller than that for LoRa. As an example, the vertical dashed lines in Fig. 1 (blue for 16-ASPM and red for 64-ASPM) indicate the maximum M-ASPM ranges if the ToA per payload must remain smaller than that for LoRa with SF $= 12$. Nevertheless, the M-ASPM maximum range under the ToA constraint can be further extended, to approach that of LoRa, by increasing M, while still providing much higher capacity than LoRa's at this range.

While the simple case of all nodes placed at the same distance from the gateway provides insights into maintaining the M-ASPM network's capacity while extending its range, it does not address a practical case of the end nodes placed over a wide area. In [2], we demonstrate that such capacity-preserving range extension can be achieved for numerous desired and/or actual areal distributions of the uplink nodes. To maintain the focus on the most essential scaling properties of M-ASPM networks, in [2] we have made a number of simplifying assumptions. In particular, we assumed transmissions with a constant average power, without discussing the effect of different PSFs on the peak-to-average power ratio (PAPR) of the modulated signal, and thus the efficiency of the power amplifier (PA). For such a constant-power transmission the range is controlled, for a given M, by the IpI (and thus the data rate) only. However, adapting to any change in the areal distribution of the nodes and/or in the propagation conditions in order to maintain the network capacity would require not only changes in the data rates of individual nodes, but also changes in the total number of the PSF channels and the number of nodes per channel. Thus a practical administration of such a network can be rather complicated, and it may become infeasible for complicated propagation environments with greatly varying path losses.

In contrast, we can greatly simplify the network planning and management if we adopt the same constant (minimal) data rate for all uplink nodes and instead control the range by changing the nodes' transmit power. Then we can maintain the total number of the PSF channels, the number of nodes per any PSF channel, as well as the total number of nodes, for any areal distribution within a given range and for various path-loss conditions. This is illustrated by the toy example below. Further, in the subsequent sections of this paper we demonstrate how such power control can be implemented, without sacrificing the PA efficiency, through the M-ASPM pulse shaping, thus enabling highly practically scalable LPWANs.

A. TOY EXAMPLE OF AREAL COVERAGE

In a wide areal coverage, different nodes may be located at substantially different distances from the gateway. For a toy example of such coverage, let us place a κ-th fraction of the nodes at distance d_1, and the rest of the nodes at $d_2 > d_1$. Then

$$\begin{cases} C_{\rm tot} = m_1\, C_1(d_1) + m_2\, C_1(d_2) \\ \dfrac{m_1}{m_2} = \dfrac{\kappa}{1-\kappa}\,\dfrac{C_1(d_2)}{C_1(d_1)}, \end{cases} \tag{6}$$

where $C_{\rm tot}$ is the total number of nodes, $C_1(d)$ is the number of nodes at the range d in a single PSF channel, and $m_1 = m(d_1)$ and $m_2 = m(d_2)$ are the numbers of the PSF channels at ranges d_1 and d_2, respectively, that can be used under the SIR constraint SIR$^{-1} \le \Delta_{\rm SIR}$ for any node.

Note that, for a given transmit power, the range d for spread-spectrum M-ASPM operation (i.e., for a sufficiently large d) is a monotonically increasing function of the IpI. In particular, for a power-law path loss with the path-loss exponent γ [4], d^γ is proportional to the IpI. At the same time, (i) under a given constraint on the co-PSF collisions, the maximum number of nodes in a single PSF channel is inversely proportional to the IpI, and (ii) if the SIR margin $\Delta_{\rm SIR}$ is defined as in [2] (also in Section II-C of this paper), $\Delta_{\rm SIR}$ is proportional to the IpI. Then $C_1(d) \propto 1/d^\gamma$ and $\Delta_{\rm SIR}(d) \propto d^\gamma$.

As a result, if all nodes transmit at the same power, $C_1(d_2)/C_1(d_1) = \Delta_{\rm SIR}(d_1)/\Delta_{\rm SIR}(d_2) = (d_1/d_2)^\gamma$ and,

to comply with the SIR constraint $\mathrm{SIR}^{-1} \leq \Delta_{\mathrm{SIR}}$ for any node, (6) can be rewritten as

$$\begin{cases} C_{\mathrm{tot}} = m_1\, C_1(d_1) + m_2\, C_1(d_2) \\ m_2 = (1-\kappa)\left(1 + \dfrac{\Delta_{\mathrm{SIR}}(d_2)}{\alpha}\right) \\ m_1 = \left(\dfrac{d_1}{d_2}\right)^{\gamma} \dfrac{\kappa}{1-\kappa}\, m_2. \end{cases} \tag{7}$$

Predictably, when the κ-th fraction of the nodes is moved from d_2 to a shorter range d_1, the number of the nodes remaining at d_2 and the number of the PSF channels deployed for those nodes is simply the $(1-\kappa)$-th fraction of the nodes and channels originally deployed at d_2. However, the number m_1 of the PSF channels at d_1, as well as the number $C_1(d_1)$ of the nodes per channel at d_1 (i.e., the data rates) vary greatly with the distance d_1 and the value of the path-loss exponent γ. In addition, even for a given d_1 and stable propagation conditions, the total number of the PSF channels (m_1+m_2) varies with the fraction κ of the nodes moved to d_1.

If, instead, we use the same interpulse interval for the nodes at d_1 as at $d_2 > d_1$, but reduce the transmit power of the nodes at d_1 by the factor $(d_1/d_2)^{\gamma}$, then

$$\begin{cases} C_{\mathrm{tot}} = (m_1 + m_2)\, C_1(d_2) \\ m_2 = (1-\kappa)\left(1 + \dfrac{\Delta_{\mathrm{SIR}}(d_2)}{\alpha}\right) \\ m_1 = \dfrac{\kappa}{1-\kappa}\, m_2, \end{cases} \tag{8}$$

and the total number of the PSF channels $(m_1 + m_2)$, the number of nodes per any PSF channel $C_1(d_2)$, as well as the total number of nodes C_{tot} remain constant for any value of d_1, any fraction κ of the nodes placed at d_1, and for any given value of the path-loss exponent γ.

Note that both the equal-power and the equal-IpI approaches in this toy example result in the same total number of the nodes C_{tot} and, if there is no efficiency penalty for controlling the transmit power, in the same total energy consumption of the nodes. However, maintaining a constant IpI while controlling the transmit power enables us to significantly simplify the management of the network in response to changes in the areal distribution of the nodes and/or in the path attenuation.

B. BEYOND TOY EXAMPLE

In a more realistic scenario, a large number of nodes would be distributed over multiple locations. If all nodes transmit with the same average power, a change in the areal distribution of the nodes and/or in the propagation conditions would generally impact both the signal-to-noise ratio (SNR) and the SIR of the mutual interference for each node. To maintain the target BER, we would then need to adjust the nodes' IpIs. However, such adjustment changes not only the nodes' SIR margins (and thus the impact of the mutual interference), but it also affects the SIR values themselves (by changing the ToA and thus the channel utilization, i.e., the values of α, for each node).

If the path loss for each node can be obtained fairly accurately, then, by solving a system of nonlinear equations and inequalities representing the interdependencies among the above quantities, we can reconfigure the network in a manner that maximizes its capacity, that is, so that all PSF channels are fully utilized. Note that it would generally require modifications in the data rates of individual nodes (i.e., in their IpIs), an update to total number of the PSF channels, and a change in the number of nodes per channel.

In contrast, if we somehow manage to adjust the transmit powers of the nodes so that their received powers remain unchanged, then the SNR and the SIR values, the SIR margins, the data rates, and the channel utilization for each node all remain the same. Consequently, there are no other changes to the network, beyond the adjustment in the nodes' transmit power.

If we are not concerned with the energy efficiency of transmissions, then the transmitted M-ASPM waveforms can be rather arbitrary. This allows us to use different IpIs and/or transmit powers for different nodes in the the same PSF channel. In practical implementations, however, we may want the signal transmitted from any node to consist of constant-envelope pulses with the same amplitude. Then, if the "idle" (i.e., for the zero-amplitude intervals between pulses) power consumption during the transmission of such a signal is negligible, then the efficiency of this transmission will be effectively the same as the efficiency of transmitting a continuous constant-envelope waveform with the same amplitude. With such a constraint on the M-ASPM waveform, only one IpI value per PSF channel can be used for constant-power transmissions, and only one transmit power setting per PSF channel can be used in the equal-IpI case. Nevertheless, for a large total number of the PSF channels, this constraint does not severely limit the effectiveness of controlling the transmit power of the M-ASPM nodes.

Our main goal in the rest of the paper is to outline a practical approach to implementing such an energy-efficient M-ASPM power control, that can be used for scaling LPWANs with realistic desired and/or actual areal distributions of the uplink nodes under different propagation conditions.

In Section II, we describe the noncoherent single-sideband M-ASPM with constant-envelope pulses, which is used in the subsequent sections of the paper. We analyze the M-ASPM's spectral efficiency, its uncoded BER performance in an AWGN channel, and the range control by the IpI when operating in the spread-spectrum region. We then discuss the SIR margins for mutual interference of multiple M-ASPM transmitters with different PSFs, and the relation of these margins to the spectral efficiency, the IpI, and the range.

In Section III, we address the M-ASPM's range and power control by changing pulse duty cycles of transmissions, and discuss the physical range comparison between LoRa and M-ASPM. We then proceed to wide areal coverage with equal-IpI M-ASPM, providing several illustrative examples

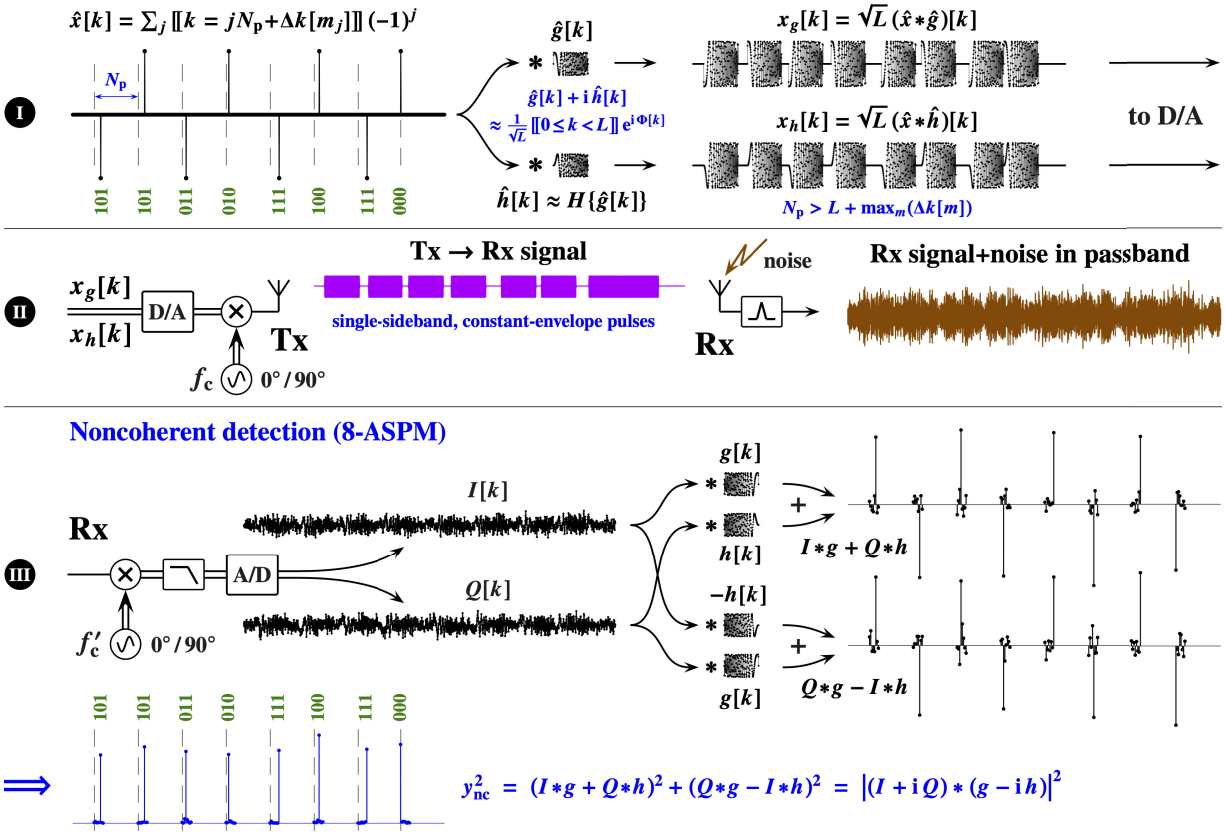

FIGURE 2. Illustration of single-sideband M-ary ASPM link with constant-envelope pulses and noncoherent detection.

and simulations for mutual interference of multiple transmitters. Further, to simplify optimization of the transmit and the received parameters of individual nodes according to their spatial locations, we introduce the node density functions for areal distributions. Such a density function characterizes the aggregate of multiple discrete node locations in terms of two continuous coordinates, for a polar coordinate system centered at the gateway.

In Section IV, we examine, for both the equal-power and the equal-IpI approaches to M-ASPM network management, how the total throughput of the uplink nodes distributed over a wide area can be maximized while M-ASPM transmissions remain constant-envelope. Further, for a uniform areal coverage beyond some range d_0 within a hexagonal cell with the circumradius $d_{\max}$, which is a basic unit for wide-area cellular coverage, we make quantitative comparisons between the equal-power and the equal-IpI arrangements. In particular, for the power-law path loss, we examine how (i) the total number of the PSF channels, (ii) the distribution of the nodes among these channels, (iii) the total number of nodes within the coverage area, and (iv) their energy efficiency, are affected by the changes in d_0, $d_{\max}$, and/or in the value of the path-loss exponent.

In Section V, we illustrate the contrast between LoRa and equal-IpI M-ASPM when both are used for wide areal coverage. Specifically, when the path loss increases with the distance from the gateway, we show that M-ASPM enables noticeably larger effective range than LoRa, combined with the flexibility of achieving various node distributions within the maximum range.

We conclude the paper with the discussion in Section VI, where we also outline a basic procedure that can be used for managing the equal-IpI M-ASPM networks without reliance on the physical location of the nodes and the path-loss models.

Henceforth, whenever we compare M-ASPM and LoRa, we assume identical physical parameters of the links. For example, we assume the same physical frequency band, transmit power, antenna gains, and various system attenuations such as insertion and matching losses, etc. Further, while the PSF length and the IpI in M-ASPM are integers, their practical values are rather large, and we routinely treat them as continuous variables, in particular, when relating them to other continuous quantities (e.g., the range).

II. NONCOHERENT SINGLE-SIDEBAND M-ASPM WITH CONSTANT-ENVELOPE PULSES

For convenience of the reader, let us first briefly describe a particular version of an M-ASPM link. This link is illustrated in Fig. 2, and it will be used in the rest of the paper. A more detailed and general M-ASPM PHY description can be found in [1], [2], and [7].

We can encode information in the "arrival times" k_j of the pulses in a digital "pulse train" $\hat{x}[k]$, where only relatively small fraction of samples have non-zero values. Such a "designed" pulse train (an example shown on the left of Fig. 2(I)) can be expressed as

$$\hat{x}[k] = \sum_j [\![k = k_j]\!] (-1)^j, \tag{9}$$

where k is the sample index, k_j is the sample index of the j-th pulse, and $[\![\ldots]\!]$ is the *Iverson bracket* [8] which is equal to 1 if the expression inside is true and 0 if it is false. The alternating signs of the pulses in (9) simply ensure that $\hat{x}[k]$ is a zero-mean signal. This helps to eliminate a direct current (DC) bias in the modulating signal, which is convenient but not strictly necessary.

For the arrival times in (9) one can use, for example,

$$k_j = jN_\mathrm{p} + \Delta N + \Delta k[m_j], \tag{10}$$

where $N_\mathrm{p} = \langle k_j - k_{j-1} \rangle$ is the average interpulse interval (IpI), ΔN is an integer, $m_j \le M$ is a positive integer, and $\Delta k[m]$ is an integer-valued invertible function such that $0 \le \Delta k[m] < N_\mathrm{p}$ and $\Delta k[m] \ne \Delta k[l]$ for $m \ne l$. The average "pulse rate" f_p in such a train is $f_\mathrm{p} = F_\mathrm{s}/N_\mathrm{p}$, where F_s is the sample rate. For $m_j \in \{1, 2, \ldots, M\}$ this pulse train encodes $\log_2 M$ bits per pulse, and thus the raw bit rate f_b is $f_\mathrm{b} = f_\mathrm{p} \log_2 M$. In the example of Fig. 2, $M = 8$ and $\hat{x}[k]$ encodes 3 bits per pulse. The corresponding 3-bit binary numbers are indicated for each pulse. Note that the peak-to-average power ratio (PAPR) of the designed pulse train $\hat{x}[k]$ is rather large, as it is equal to the IpI $N_\mathrm{p} \gg 1$, and this train would be unsuitable for modulating a carrier.

However, the high-PAPR train $\hat{x}[k]$ given by (9) can be "reshaped" by linear filtering, creating a lower-PAPR modulating signal. In particular, the impulse response $\hat{\zeta}_i[k]$ of such a "pulse shaping" filter (PSF) can be a nonlinear chirp with the desired autocorrelation function (ACF), e.g.

$$\hat{\zeta}_i[k] = \hat{g}_i[k] + \mathrm{i}\,\hat{h}_i[k] = \frac{1}{\sqrt{L_i}} [\![0 \le k < L_i]\!] \exp\left(\mathrm{i}\,\Phi_i[k]\right), \tag{11}$$

where $\Phi_i[k]$ is the phase and L_i is the "duration" (length) of the chirp in samples. In (11), the imaginary part of $\hat{\zeta}_i[k]$ is the discrete Hilbert transform of its real part, i.e., $\hat{h}_i[k] = H\left\{\hat{g}_i[k]\right\}$ [9], [10]. For the i-th PSF $\hat{\zeta}_i[k]$, we will denote its matched filter $\hat{\zeta}_i^*[-k] = \hat{g}_i[-k] - \mathrm{i}\,\hat{h}_i[-k]$ by removing the overhead hat symbol, as $\zeta_i[k] = \hat{\zeta}_i^*[-k]$.

Filtering the designed train $\hat{x}[k]$ with the PSF $\hat{\zeta}_i[k]$ creates the digital modulating signal $z_i[k]$ ("reshaped train")

$$z_i[k] = \sqrt{L_i}\,(\hat{x} * \hat{\zeta}_i)[k] = \sqrt{L_i} \sum_j \hat{\zeta}_i[k - k_j], \tag{12}$$

where $\hat{\zeta}_i[k]$ is given by (11) and the asterisk denotes convolution. Since in Fig. 2 we show only a single PSF channel, in the figure we omit the subscript i, and also denote the real and imaginary parts of $z[k]$ as $x_g[k]$ and $x_h[k]$, respectively.

After digital-to-analog (D/A) conversion, the real and imaginary parts of $z_i(t)$ can be used for quadrature amplitude modulation of a carrier with frequency f_c, providing the transmitted waveform $\mathrm{Re}(z_i(t))\sin(2\pi f_\mathrm{c} t) + \mathrm{Im}(z_i(t))\cos(2\pi f_\mathrm{c} t)$. Since $\hat{h}_i[k]$ is the Hilbert transform of $\hat{g}_i[k]$, this waveform will occupy only a single sideband with the physical bandwidth B equal to the baseband bandwidth of $\hat{\zeta}_i[k]$ [9]. In addition, if the chirps in (12) do not overlap (i.e., $L_i \le N_\mathrm{p} - \max_m(\Delta k[m])$), then

$$|z_i[k]| = \sum_j [\![0 \le k - k_j < L_i]\!], \tag{13}$$

and, as illustrated in Fig. 2(II), the transmitted signal will consist of constant-envelope pulses. Note that the variance of such a reshaped train is equal to L_i/N_p, and thus, for a given IpI N_p, the average power of $z_i[k]$ is proportional to L_i.

For noncoherent ('nc') detection (Fig. 2(III)), in the receiver's (Rx) quadrature demodulator the noisy passband signal is multiplied by the orthogonal sinusoidal signals from a local oscillator, lowpassed, and converted to the in-phase and quadrature digital signals $I[k]$ and $Q[k]$. We can then use the matched filters $g[k]$ and $h[k]$, as shown in Fig. 2(III), to obtain the high-peakedness pulse train $y_\mathrm{nc}[k]$ corresponding to the designed pulse train. Note that after synchronization we would need to obtain only $M = 8$ samples per pulse, i.e., we can use $g[k]$ and $h[k]$ as decimation filters. Out of each 8 samples of $y_\mathrm{nc}[k]$, the position of the sample with the largest magnitude will correspond to the position of the respective pulse in the designed train.

A. M-ASPM SPECTRAL EFFICIENCY

Without noise, the received pulse train $y_\mathrm{nc}[k]$ will be proportional to the convolution of the designed train $\hat{x}[k]$ with the ACF of the PSF. Thus, as discussed in [1] and [2], a good choice for the ACF would be a pulse that combines a small time-bandwidth product (TBP) [11], [12] (e.g., close to that of a Gaussian pulse) with a compact frequency support. An example of such ACF would be a raised-cosine (RC) pulse [13] with a sufficiently large roll-off factor $0 \le \beta \le 1$. Then the sample rate F_s in the digital waveforms can be chosen as $F_\mathrm{s} = 2\mathcal{N}_\mathrm{s} B$, where $1 \le \mathcal{N}_\mathrm{s} = 2/(1+\beta) < 2$ is the oversampling factor.

From now on, to distinguish between the respective quantities for LoRa and M-ASPM, let us mark those for LoRa by overhead tildes. Then the spectral efficiency of LoRa modulation is

$$\widetilde{\eta} = \widetilde{\eta}\left(\widetilde{M}\right) = \frac{\log_2 \widetilde{M}}{\widetilde{M}}. \tag{14}$$

If we use PSFs with RC ACFs, and the sample rate $F_\mathrm{s} = 4B/(1+\beta)$, then for M-ASPM operating in the spread-spectrum region

$$\eta = \eta\left(M, N_\mathrm{p}\right) = \frac{4\log_2 M}{(1+\beta)N_\mathrm{p}} = \widetilde{\eta}(M)\,\frac{4M}{(1+\beta)N_\mathrm{p}}, \tag{15}$$

and, for a given M, the spectral efficiency is inversely proportional to the IpI N_p. For example, with $\beta = 1/3$, $\eta = 12/N_\mathrm{p}$

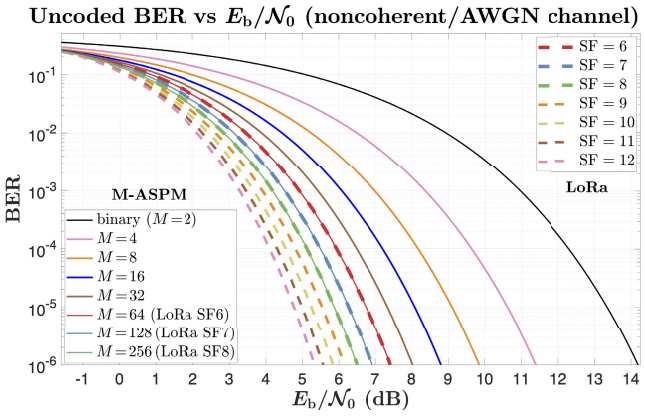

FIGURE 3. Uncoded BER vs $E_b/\mathcal{N}_0$ performances of LoRa (dashed lines) and single-sideband M-ASPM (solid lines) for noncoherent detection in AWGN channel.

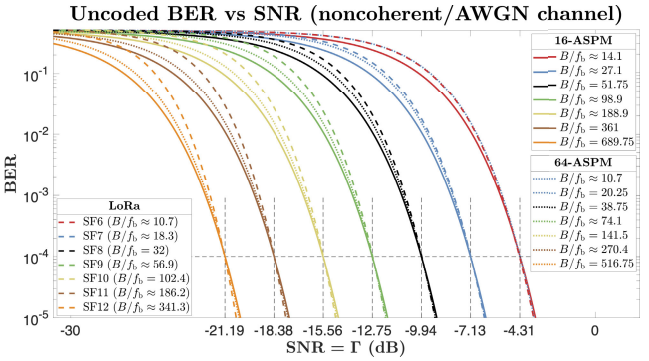

FIGURE 4. Uncoded BER vs SNR performances of LoRa (dashed lines), single-sideband 16-ASPM (solid lines), and single-sideband 64-ASPM (dotted lines) for noncoherent detection in AWGN channel.

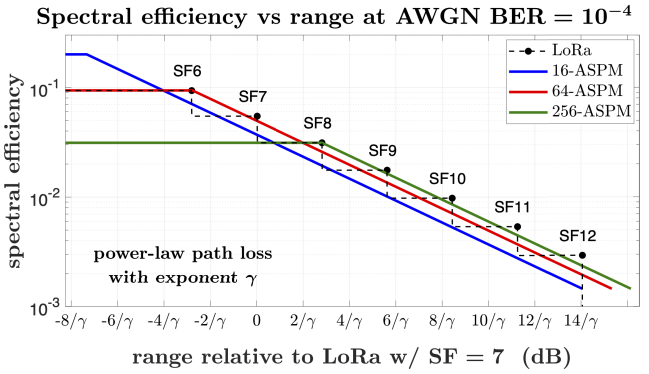

FIGURE 5. Spectral efficiency vs range for LoRa and M-ASPM (noncoherent detection).

for $M = 16$, and $\eta = 24/N_p$ for $M = 64$. The minimum N_p value that can be used in noncoherent M-ASPM is $4M$, and thus the maximum spectral efficiency of M-ASPM is

$$\eta_{\max} = \eta\,(M, 4M) = \widetilde{\eta}(M)/(1+\beta). \tag{16}$$

Note that, when $\beta = 0$ (sinc function ACF), it is equal to the spectral efficiency of noncoherent LoRa with $\widetilde{M} = M$.

B. UNCODED BER PERFORMANCE OF M-ASPM IN AWGN CHANNEL AND RANGE CONTROL BY Ipl

While AWGN is only a "background" noise in most practical LPWAN applications, the performance in an AWGN channel provides a suitable benchmark for the M-ASPM's overall efficiency assessment and for examining its main scaling properties.

As a reminder (see [1], [2]), for noncoherent M-ASPM the bit error probability P_b in AWGN channel can be expressed as

$$P_b = P_b\left(\frac{\Gamma}{\eta}\right) = \frac{1}{2(M-1)}\sum_{k=2}^{M}(-1)^k\binom{M}{k}\exp\left(-\frac{k-1}{k}\,\frac{\Gamma}{\eta}\,\log_2 M\right), \tag{17}$$

where $\binom{n}{m} = \frac{n!}{(n-m)!\,m!}$ is the binomial coefficient, Γ is the SNR, and $\eta = f_{b/B}$ is the spectral efficiency. The SNR can be further expressed as $\Gamma = (E_b/\mathcal{N}_0) \times (f_b/B)$, where E_b is the energy per bit and $\mathcal{N}_0$ is the (one-sided) power spectral density (PSD) of the noise. Notably, as illustrated in Fig. 3, the AWGN bit error probability for M-ASPM is the same as for noncoherent LoRa when $M = 2^{SF}$ [6].

If we desire to achieve the same BER performance at the same range (i.e., at the same Γ) for LoRa (with a given $\widetilde{M}$) and M-ASPM (with a given M), the value of η (and thus N_p) can be obtained as a solution of the equalities

$$P_b\left(\Gamma; M, N_p\right) = \widetilde{P}_b\left(\Gamma; \widetilde{M}\right) = \text{BER}. \tag{18}$$

An example is given in Fig. 4 for M-ASPM with $M = 16$ and $M = 64$, and BER $= 10^{-4}$.

Normally, the received power decreases with the distance d between the transmitter and the receiver, and the SNR is a decreasing function of d. For example, for the power-law path loss $\Gamma \propto d^{-\gamma}$, where γ is the path-loss exponent. For free-space path loss $\gamma = 2$, and it can be 2-3 times larger for harsh environments [14], [15], [16], [17]. Then, from the condition $\Gamma/\eta = const$ it follows that, for the power-law path loss, the M-ASPM range $d \propto \eta^{-1/\gamma} \propto {N_p}^{1/\gamma}$. This is in contrast with LoRa, where LoRa's spectral efficiency is constant for a given spreading factor. While N_p is an integer, it is rather large ($N_p \geq 4M$ for noncoherent M-ASPM) and, for a sufficiently large M (e.g., $M \geq 16$), the M-ASPM's spectral efficiency can be treated as a continuous quantity. For example, Fig. 5 illustrates M-ASPM's spectral efficiency vs. range under power-law path loss model, at AWGN BER $= 10^{-4}$, as compared with LoRa. For M-ASPM, for the spectral efficiencies larger than $(\log_2 M)/M$ the value of η is obtained as the solution of the equality $P_b\,(d; M, \eta) =$ BER. For LoRa, the spectral efficiency is the maximum value of $\widetilde{\eta}$ satisfying the inequality $\widetilde{P}_b\,(d; \widetilde{\eta}) \leq$ BER.

C. SIR MARGINS FOR MUTUAL INTERFERENCE OF M-ASPM TRANSMITTERS WITH DIFFERENT PSFs

When considering the impact of mutual interference of multiple M-ASPM transmitters, we shall recall that different

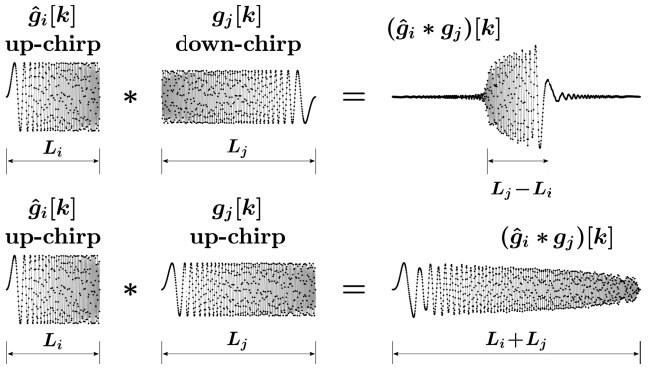

FIGURE 6. For sufficiently different L_i and L_j, cross-correlations of $\hat{g}_i[k]$ and $\hat{g}_j[k]$ for constant-envelope PSFs given by (11) will have large TBPs.

M-ASPM transmitters can employ substantially different PSFs, in a manner similar to using different spreading sequences in asynchronous code-division multiple access (CDMA) [18].

As discussed in [2], one can construct many PSFs, $\hat{\zeta}_1[k]$, $\hat{\zeta}_2[k]$, and so on, with large-TBP components $\hat{g}_i[k]$ such that they have the same small-TBP ACF $w[k]$, i.e., $(\hat{g}_i * g_i)[k] = w[k]$ for any i, while the convolutions of any $\hat{g}_i[(t)]k]$ with $g_j[(t)]k]$ for $i \neq j$ (cross-correlations) have large TBPs. Then the impact of the interference from transmitters with $\hat{\zeta}_j[k] \in \{\hat{\zeta}_2[k], \hat{\zeta}_3[k], \dots\}$ (i.e., when $j \neq 1$) on the signal from the transmitter with $\hat{\zeta}_1[k]$ would be akin to the impact of a noise with relatively low PAPR and the power equal to the combined power of the interfering signals at the receiver. While such noise is non-Gaussian in general, its Gaussian approximation would be mostly adequate for the assessment of its effect on the BER, especially at low SNRs [19].

In particular, let us consider constant-envelope PSFs with the impulse response expressed by (11). Then, for sufficiently different L_i and L_j (e.g., for $|L_i - L_j| \gg \mathcal{N}_s$, where $\mathcal{N}_s$ is the oversampling factor), cross-correlations of $\hat{g}_i[k]$ and $\hat{g}_j[k]$ will always have large TBPs. This is illustrated in Fig. 6.

If the interference with a given SIR can be treated as Gaussian contribution to the noise, then its impact can be quantified by the deterioration (increase) in the AWGN BER from a given BER value to BER$' >$ BER, when the SNR Γ becomes the signal-to-interference-plus-noise ratio (SINR) $\Gamma' < \Gamma$:

$$P_b\left(\frac{\Gamma}{\eta}; M\right) = \mathrm{BER} = P_b\left(\frac{\Gamma'}{\eta}; M\right)\frac{\mathrm{BER}}{\mathrm{BER}'}. \tag{19}$$

By solving (19) for the given M, BER, and BER$'$, we can obtain the (constant) values of Γ/η and Γ'/η. Consequently, for a given spectral efficiency η, we can express the *SIR margin* Δ_{SIR} as

$$\Delta_{\mathrm{SIR}} = \frac{1}{\Gamma'} - \frac{1}{\Gamma} = \left(\frac{\eta}{\Gamma'} - \frac{\eta}{\Gamma}\right)\eta^{-1} = \eta^{-1} \times const, \tag{20}$$

and thus the SIR margin for M-ASPM is inversely proportional to its spectral efficiency or, equivalently, to the IpI: $\Delta_{\mathrm{SIR}} \propto \eta^{-1} \propto N_p$. For $M = 16$ and $M = 64$, Fig. 7 illustrates the range of values for the product $\eta\,\Delta_{\mathrm{SIR}}$, in relation to the chosen constraints on BER and BER$'$.

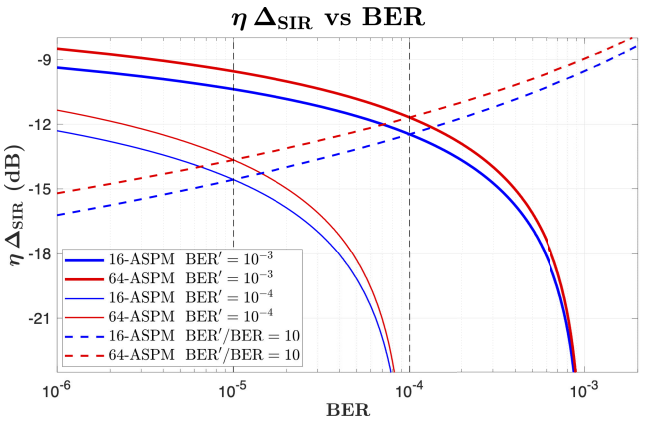

FIGURE 7. Product $\eta\,\Delta_{\mathrm{SIR}}$ in relation to chosen constraints on BER and BER$'$.

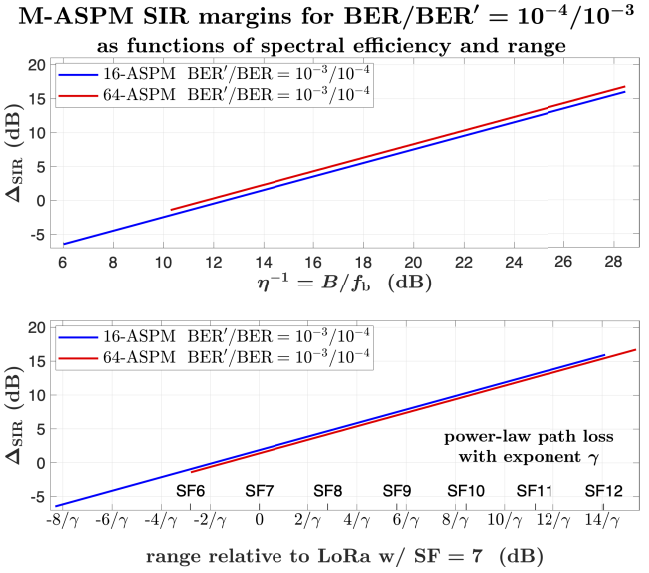

FIGURE 8. SIR margins for inter-PSF interference in M-ASPM scale as $\Delta_{\mathrm{SIR}} \propto \eta^{-1} \propto N_p$, and for power-law path loss as $\Delta_{\mathrm{SIR}} \propto d^{\gamma}$.

Further, when an M-ASPM node transmits at the spectral efficiencies below the maximum for a given M (that is, in the spread-spectrum region), both its inverse spectral efficiency η^{-1} and its range d increase with the IpI N_p. In particular, for a power-law path loss with the path-loss exponent γ [4], d^{γ} is proportional to the IpI. Then

$$\Delta_{\mathrm{SIR}} \propto \eta^{-1} \propto N_p \propto d^{\gamma}. \tag{21}$$

This is illustrated in Fig. 8 for M-ASPM with $M = 16$ and $M = 64$, for BER$'$/BER $= 10^{-3}/10^{-4}$.

III. RANGE AND POWER CONTROL BY PULSE DUTY CYCLE

For a given pulse amplitude, the average transmit power of an M-ASPM signal with constant-envelope pulses is proportional to L/N_p, where L is the length of the pulse and N_p is the IpI. We shall call the ratio $D = L/N_p < 1$ a *pulse duty cycle*, and thus the average transmit power is proportional to D.

If the "idle" (i.e., for the zero-amplitude intervals between pulses) power consumption during the transmission of such a signal is negligible, then the efficiency of this transmission is effectively the same as the efficiency of transmitting a continuous constant-envelope waveform with the same amplitude. Therefore, for a given *peak* transmit power of an M-ASPM signal, the *average* transmit power can be controlled by the pulse duty cycle without sacrificing the transmission efficiency.

As follows from (17), for a given M, the same uncoded BER in an AWGN channel for two M-ASPM transmitters will be achieved when $\Gamma_1/\eta_1 = \Gamma_2/\eta_2$, where, respectively for the first and the second transmitter, Γ_1 and Γ_2 are the SNRs, and η_1 and η_2 are the spectral efficiencies. Then, for two otherwise identical transmitters (i.e., having the same PSF ACF and operating in the same frequency band, with the same antenna gains, various system attenuations, etc.) that are placed at the distances d_1 and d_2 from the receiver and transmit with different average powers, the same BER will be achieved when

$$\frac{P_1(d_1)}{P_2(d_2)} = \frac{\eta_1}{\eta_2} = \frac{N_2}{N_1}, \tag{22}$$

where $P_1(d_1)$ and $P_2(d_2)$ are the respective *received* powers, and N_1 and N_2 are the respective IpIs.

Note that in the absence of noise the equal-BER condition expressed by (22) signifies the equality of the magnitude of the pulses in the received pulse trains $y^2_{\mathrm{nc}}[k]$ for the first and the second transmitter. When the noise is present, we can transmit a payload comprising a sufficiently long sequence of pulses with the same position offsets. Then, for the time interval specific to transmitting such a "gauge" payload, the magnitude of the "noise-free" pulses can be accurately measured by using the *modulo power averaging* (MPA) function described in [20], where it is used for reliable, even at extremely low SNRs, synchronization of the pulse trains in the receiver. Consequently, by measuring the received pulse magnitudes for a pair of nodes placed at different locations, we can determine the relative path loss for these nodes and monitor its time fluctuations in dynamically changing propagation conditions. As demonstrated in [20], the MPA also allows to directly obtain the receiver's baseband SINR, with the accuracy not significantly affected by the co-PSF collisions.

Such measurements of the received pulse magnitudes can be performed for multiple nodes, with the node locations and the frequency of the measurements depending on the complexity of the environment and the desired precision. These measurements can then be extrapolated to "map" the path loss for the area specific to the gateway. Throughout this paper, however, we use the simple power-law path loss model, which is adequate for illustration of the main scaling properties of M-ASPM, and for its comparison with LoRa.

For the power-law path loss with the path-loss exponent γ, the average received power P at a distance d from the transmitter can be approximated as

$$P(d) = P(d_0)\left(\frac{d_0}{d}\right)^{\gamma}, \tag{23}$$

where $P(d_0)$ is the power received at a reference point in the far field region at the distance d_0 from the transmitter. With (23), the condition (22) can be rewritten as

$$\frac{P_1(d_1)}{P_2(d_2)} = \frac{P_1(d_0)}{P_2(d_0)}\left(\frac{d_2}{d_1}\right)^{\gamma} = \frac{N_2}{N_1}. \tag{24}$$

Since the received powers $P_1(d_0)$ and $P_2(d_0)$ are for the same distance d_0 from the transmitters, their ratio is identical to the ratio of the respective *transmit* powers. Consequently, the same BER in an AWGN channel will be achieved for the transmitters placed at the distances d_1 and d_2 when

$$\left(\frac{d_1}{d_2}\right)^{\gamma} = \frac{D_1 N_1}{D_2 N_2}, \tag{25}$$

where D_1 and D_2 are the pulse duty cycles for the first and the second transmitter, respectively.

Therefore, for transmission with a constant peak power and a given IpI, the average transmit power is proportional to the pulse duty cycle D, and the range d increases with D (e.g., as $d \propto D^{1/\gamma}$ for the power-law path loss).

A. PHYSICAL RANGE

Since the path loss is highly dependent on the environment, a generic value for the communication range cannot be given. Instead, we can quantify a physical range of an M-ASPM transmitter in terms of the range of some "standard" (benchmark) transmitter operating under effectively the same physical conditions. For example, we can use LoRa with SF = 7 ($\widetilde{M} = 2^7 = 128$) as a particular choice of such benchmark transmitter. In fact, the range of LoRa with SF = 7 has been used as the benchmark "intermediate" range in our preceding discussions of the M-ASPM range-related properties (e.g., in Figs. 1, 5, and 8). We shall denote this range as δ_0. For the subsequent numerical results of this paper, we will use an AWGN channel and calculate $\widetilde{\delta_0}$ for the uncoded BER $= 10^{-4}$. Further, we will still assume the power-law path loss, and thus $\widetilde{\delta_0}$ is a function of the path-loss exponent, $\widetilde{\delta_0} = \widetilde{\delta_0}(\gamma)$.

With this, the range of an M-ASPM transmitter can be expressed as

$$d = \left(D\,\frac{\eta_0}{\eta}\right)^{1/\gamma}\widetilde{\delta_0}(\gamma), \tag{26}$$

where D is the pulse duty cycle, η is the spectral efficiency, and the value of η_0 can be obtained by solving $P_{\mathrm{b}}(\Gamma; M, \eta_0) = \widetilde{P}_{\mathrm{b}}(\Gamma; 128) =$ BER. For example, as can be seen in Fig. 4, $\eta_0 = 1/27.1$ for 16-ASPM, and $\eta_0 = 1/20.25$ for 64-ASPM.

Note that in Figs. 1, 5, and 8, as well as in the remainder of this paper, the LoRa ranges for other spreading factors (i.e., SF $\neq$ 7) are also expressed in relation to $\widetilde{\delta_0}(\gamma)$.

B. WIDE AREAL COVERAGE WITH CONSTANT IpI

As illustrated in the toy example of Section I-A for two distinct ranges, we can significantly simplify the management of an M-ASPM network if we maintain the same IpI for all nodes and, instead, adjust the nodes' transmit power to ensure the equality of the received powers for all nodes. In this example, however, for a large total number of the PSF channels, multiple PSF channels are deployed at a given range. Unfortunately, the same range for a given IpI suggests the same average transmit power. Therefore, if we require the same amplitude of constant-envelope pulses, we cannot deploy multiple (i.e., more than two) PSF channels at the same range.

Favorably, in a practical wide area network, the number of nodes greatly exceeds the number of the PSF channels, and the nodes are distributed over multiple distances from the gateway. Thus we can use the same IpI for all nodes, yet different PSF channels for different ranges. Then, as discussed below, we can control the transmit power by adjusting the channels' pulse duty cycles, while preserving the amplitude of the received pulses.

For a given IpI $N_{\rm p}$ (and thus the data rate) of an M-ASPM with constant-envelope pulses, the maximum range is achieved for the maximum pulse duty cycle $D_{\max} = 1 - \max_m(\Delta k[m])/N_{\rm p}$ (see the PSF description in Section II). For the nodes placed at shorter distances from the receiver, the pulse duty cycles can be reduced, while still satisfying the constraint on the maximum allowed uncoded BER. Then, as discussed in Section II-C, for sufficiently different pulse duty cycles the impact of the mutual interference among the transmitters would be akin to the impact of a noise with a relatively low PAPR and the power equal to the combined average power of the received interfering signals. Consequently, the number and the placement of the additional nodes within the maximum range will be constrained by the requirement that the inverse SIR of any node remains below the SIR margin $\Delta_{\rm SIR}$ (which is the same for all nodes with the same IpI).

In order to increase the maximum range under a given constraint on the transmit power, we need to increase the IpI, and thus proportionally reduce the data rate. However, since $\Delta_{\rm SIR}$ is proportional to the IpI, the reduction in the data rate of the nodes can be counteracted by the respective increase in the number of additional nodes placed at shorter ranges, thus approximately preserving the total throughput of the network. This is illustrated in Fig. 9, where the reduction in the data rate in order to extend the range is accompanied by the increase in the number of additional nodes placed at smaller distances within the range (i.e., by the increase from four to eight additional nodes).

In Fig. 9, we also illustrate the impact of mutual interference for multiple equal-IpI M-ASPM transmitters, placed at different distances from the receiver, on their received pulse trains. To highlight the impact of the interference only, there is no external noise, and thus SINR = SIR. For the specific ranges shown in the figure, the free-space path loss ($\gamma = 2$) is assumed. For this path loss and distances, the values of the pulse duty cycles for the nodes are chosen in such a way that the average powers of the received pulse trains, and thus the magnitudes of the pulses in these trains, are identical in the absence of interference. In particular, the values of the pulse duty cycles and the distances from the receiver satisfy the relation $D_i/D_j = (d_i/d_j)^\gamma$ for any pair of nodes. The magnitudes of the interference-free pulses are indicated, for each received train, by the horizontal dashed lines in the right-hand side of the figure.

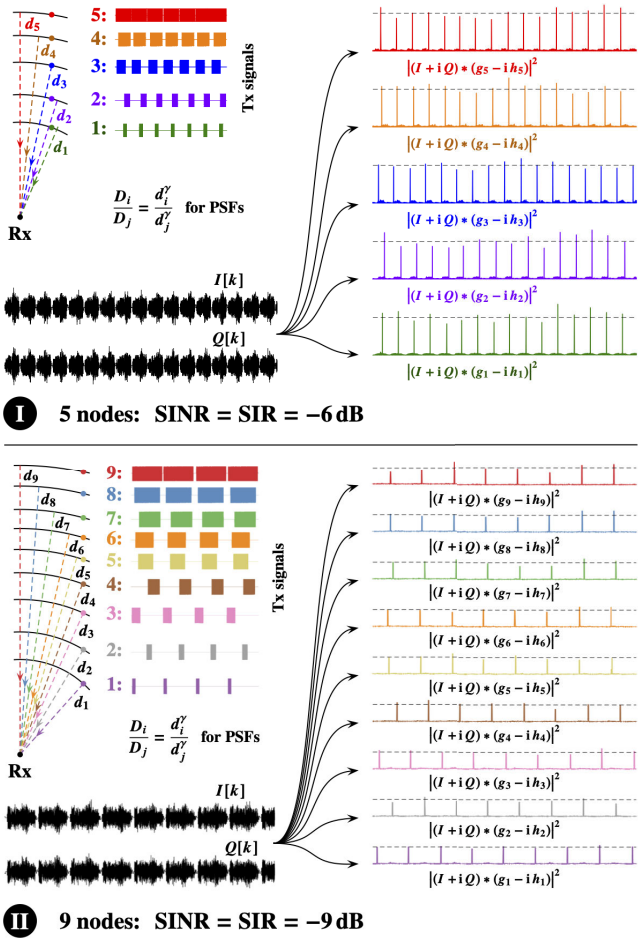

FIGURE 9. Illustration of impact of inter-PSF interference for five and nine 16-ASPM transmitters placed at particular distances from receiver. Pulse duty cycles are chosen to ensure equality of received powers, and thus for continuous transmissions SIR = −6 dB for five nodes and SIR = −9 dB for nine nodes. Specific ranges shown are for free-space path loss ($\gamma = 2$), and IpI for 9 nodes is twice that for 5 nodes.

Since the average received powers are identical, the SIR will be the same for all transmitters. For example, SIR = −6 dB for five nodes (Fig. 9(I)), and SIR = −9 dB for nine nodes (Fig. 9(II)). Further, for a given IpI the SIR margins for the nodes are also identical. Consequently, as can be seen in the figure, the mutual interference has similar impact on the magnitudes of the pulses in the received pulse trains for all nodes.

To generate the waveforms shown in Fig. 9, we used PSFs with the ACF as an RC pulse with the roll-off factor $\beta = 1/4$,

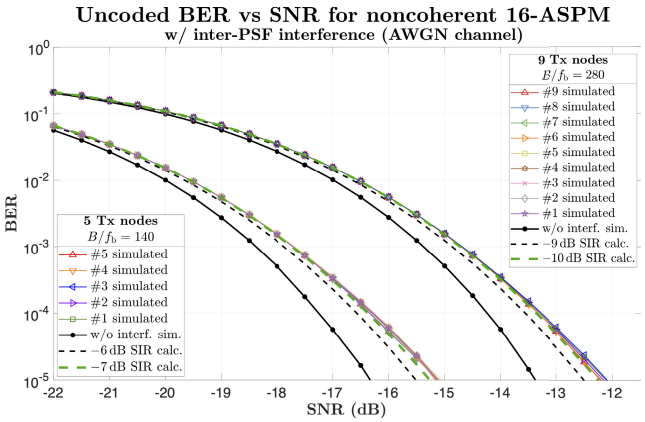

FIGURE 10. Impact of mutual interference on uncoded BER in AWGN channel for arrangements shown in Fig. 9.

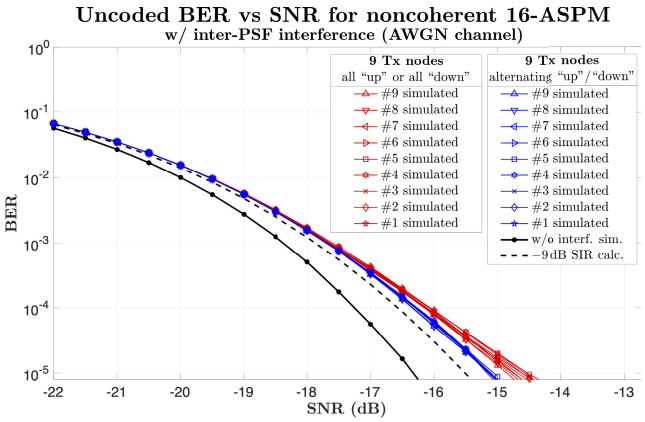

FIGURE 11. Using all "up" or all "down" chirps for PSFs with different pulse duty cycles further increases impact of mutual interference, as compared with its Gaussian approximation, and should be avoided.

and oversampling with $\mathcal{N}_s = 2/(1+\beta) = 8/5$. Further, we used noncoherent 16-ASPM ($M = 16$), and thus $\eta = f_b/B = 2\mathcal{N}_s \log_2 M/N_p = 12.8/N_p$. Specifically, to encode 4-bit sequences $(a_1b_1c_1d_1\, a_2b_2c_2d_2 \ldots a_jb_jc_jd_j \ldots)$, we used the designed pulse trains expressed by

$$\hat{x}[k] = \sum_j [\![k = jN_p + (8a_j + 4b_j + 2c_j + d_j)n]\!], \qquad (27)$$

where $n = 4$. With this, the maximum pulse duty cycle is $D_{max} = 1 - 60/N_p$. For the particular IpI value N_p used in Fig. 9(I) $\eta = 1/140$, $D_{max} = 96.7\%$, and the SIR margin for $\mathrm{BER}'/\mathrm{BER} = 10^{-3}/10^{-4}$ is $\Delta_{SIR} = 9$ dB. In Fig. 9(II), $\eta = 1/280$, $D_{max} = 98.3\%$, and $\Delta_{SIR} = 12$ dB. The minimum range in Fig. 9 is $d_1 = \widetilde{\delta}_0(2)$, for $D_1 = 20\%$ in the upper panel (I) and $D_1 = 10\%$ in the lower panel (II). The maximum ranges are $d_5 = 2.2\,\widetilde{\delta}_0(2)$ in Fig. 9(I), and $d_9 = 3.1\,\widetilde{\delta}_0(2)$ in Fig. 9(II), both for the pulse duty cycle 93.8%.

Further, for the arrangements shown in Fig. 9, Fig. 10 quantifies the impact of the mutual interference on the uncoded BER in an AWGN channel. In the simulations, the BER for a given transmitter is determined by comparing the bit sequences extracted from the "ideal" transmitted signal (without noise and interference), and from the transmitted signals affected by an AWGN only (black dots connected by black solid lines), and by an AWGN and the signals from all other transmitters (colored markers connected by solid lines).

As was discussed earlier, when different nodes employ sufficiently different pulse duty cycles, a Gaussian approximation for the mutual interference is adequate for a rough assessment of its effect on the BER. These calculated Gaussian approximations are shown in Fig. 10 by the black dashed lines, and they indeed roughly correspond to the simulated BER values. However, while the mutual interference is a low-PAPR signal, it is still a super-Gaussian rather than a Gaussian signal [19], which results in its somewhat higher impact on the BER as compared to the impact of a Gaussian noise. As a consequence, in Fig. 10 the simulated BER values are much better approximated by the "effective" Gaussian interference, which is about 1 dB higher in both cases of four and eight interfering transmitters (green dashed lines in Fig. 10).

In order to lower the peakedness of the mutual interference, and thus its excessive impact on the BER, we would want to maximize the TBPs of cross-correlations for the PSF. Thus, as a rule of thumb, we want to alternate "up-chirp" and "down-chirp" PSFs when reducing the pulse duty cycles for the closer-range nodes. This was done in the examples of Figs. 9 and 10. Using all "up" or all "down" chirps in the PSFs with different pulse duty cycles would further increase the impact of the mutual interference, as compared with its Gaussian approximation. This is illustrated in Fig. 11, for the nine-node arrangement shown in the lower panel (II) of Fig. 9.

C. NODE DENSITY FUNCTIONS FOR AREAL DISTRIBUTIONS

In a design of a practical network, we may be given the coordinates of the end nodes placed at the desired locations, e.g., sensors co-located with traceable physical assets. In general, these coordinates can be time-variant, but we may initially assume that they vary sufficiently slowly and can be considered stationary during the ToA of any transmission. For a given placement of a gateway, the locations of the end nodes can be characterized by the distribution (density) function expressed in polar coordinates centered at the gateway, $\Phi(\varphi, r)$, where φ is the angular coordinate and $r > 0$ is the distance from the gateway [2]. It is convenient to normalize $\Phi(\varphi, r)$ to unity as

$$\int_0^{2\pi} d\varphi \int_0^{\infty} dr\, r\, \Phi(\varphi, r) = 1, \qquad (28)$$

and such normalization will be assumed in the rest of the paper.

The main purpose for introducing such a density function is to characterize the aggregate of multiple node locations by a function of two *continuous* variables, φ and r. This simplifies optimization of the transmit and received parameters of the nodes according to their spatial positions. For example, if $f(\varphi, r)$ is a physical property of the node (e.g., its transmit

or received power, ToA, data rate, etc.) that may depend on the coordinates φ and r, then its average value within some area A can be expressed as

$$\langle f(\varphi, r)\rangle_A = \frac{\iint_A d\varphi dr\, r f(\varphi, r)\, \Phi(\varphi, r)}{\iint_A d\varphi dr\, r\, \Phi(\varphi, r)}. \tag{29}$$

The reason why a physical parameter of a node may depend on the location is the path loss. For example, for a given transmit power the received power depends on this loss. Or, for a given maximum allowed uncoded BER, the IpI and/or the pulse duty cycle can be adjusted according to the propagation losses, thus making them dependent on the node's placement.

In general, the path loss may depend on the angular coordinate φ, as there may be obstacles in a certain direction from the receiver, or different multipath conditions. It also may not be a monotonic function of the distance from the receiver, or even a single-valued function of the coordinates. For example, for two transmitters in close physical proximity, one can be indoors, and the other one outdoors, which may result in significantly different path losses. However, for simplicity, in this paper we assume that (i) the path loss is independent of the direction φ and is a function of only the distance r from the gateway, and (ii) the path loss is a monotonically increasing function of r. Then the physical parameters of a node also will be functions of r only, and (29) simplifies to

$$\langle f(r)\rangle_i = \frac{\int_{d_{i-1}}^{d_i} dr\, f(r)\, \phi(r)}{\int_{d_{i-1}}^{d_i} dr\, \phi(r)}, \tag{30}$$

where the average is for the range interval $[d_{i-1}, d_i]$, and where $\phi(r)$ is the radial node density

$$\phi(r) = r \int_0^{2\pi} d\varphi\ \Phi(\varphi, r). \tag{31}$$

Note that in the toy example of Section I the radial density function is

$$\phi(r) = \kappa\, \delta(r - d_1) + (1 - \kappa)\, \delta(r - d_2), \tag{32}$$

where $\delta(x)$ is the Dirac δ-function [21].

IV. CONTRAST BETWEEN EQUAL-POWER AND EQUAL-IpI ARRANGEMENTS

Let us now examine, for both the equal-power and the equal-IpI approaches to M-ASPM network management, how the total throughput of the uplink nodes distributed over a wide area can be maximized while M-ASPM transmissions remain constant-envelope. We will assume that all nodes in a given areal coverage carry the same data payload per unit time, and are divided into m "PSF channels" such that, for any "channel index" $i \in \{1, 2, \ldots, m\}$, all nodes in the i-th channel have the same settings (i.e., the same PSF, IpI, and transmit power). Further, let all nodes be confined to the range interval $[d_0, d_{\max}]$, that is

$$\phi(r) \equiv \phi(r)\, [\![d_0 \le r \le d_{\max}]\!], \tag{33}$$

and all nodes for the i-th channel be placed within the interval $[d_{i-1}, d_i]$, where $d_0 \le d_{i-1} < d_i \le d_m = d_{\max}$.

For equal-payload nodes with the co-PSF constraint α, and the power-law path loss, the constraints on the impact of inter-PSF collisions can be expressed as

$$\langle \mathrm{SIR}\rangle_i^{-1} = \frac{\sum_{j=1}^m \frac{L_j}{N_j} \langle r^{-\gamma}\rangle_j}{\frac{L_i}{N_i} \langle r^{-\gamma}\rangle_i} - 1 \lesssim \frac{\Delta_{\mathrm{SIR}}(N_i)}{\alpha} = \frac{N_i}{\alpha\, N_{0\mathrm{dB}}} \tag{34}$$

for any $i \in \{1, 2, \ldots, m\}$, where N_i is the IpI, L_i is the length of the PSF, the average is defined by (30), and where $N_{0\mathrm{dB}}$ is such that $\Delta_{\mathrm{SIR}}(N_{0\mathrm{dB}}) = 1$ (i.e., $N_{0\mathrm{dB}} = \Delta_{\mathrm{SIR}}^{-1}(1)$).

Further, to ensure that all m PSF channels are fully utilized (i.e., they all operate at the co-PSF constraint α), for a given radial node density $\phi(r)$ the following condition must be satisfied:

$$N_i \int_{d_{i-1}}^{d_i} dr\, \phi(r) = N_j \int_{d_{j-1}}^{d_j} dr\, \phi(r) \tag{35}$$

for any $i, j \in \{1, 2, \ldots, m\}$.

If all nodes transmit at the same average power, then $N_i \propto d_i^\gamma$ and the condition (35) becomes

$$d_i^\gamma \int_{d_{i-1}}^{d_i} dr\, \phi(r) = d_j^\gamma \int_{d_{j-1}}^{d_j} dr\, \phi(r). \tag{36}$$

By solving the system of nonlinear equations represented by (36), we can then obtain the partition ranges d_i and the interpulse intervals N_i. Note that a change in the value of the path-loss exponent γ will result in a change in the partition ranges, and thus in "reassignment" of some nodes to different PSF channels. Further, for equal-power transmissions the duty cycles L_i/N_i for all channels are equal to each other, and the inter-PSF constraint (34) can be expressed as

$$\frac{N_m}{N_i} \langle \mathrm{SIR}\rangle_i^{-1} = \frac{\sum_{j=1}^m \left\langle \left(\frac{d_m}{r}\right)^\gamma \right\rangle_j}{\left\langle \left(\frac{d_i}{r}\right)^\gamma \right\rangle_i} - \left(\frac{d_m}{d_i}\right)^\gamma \lesssim \frac{N_m}{\alpha\, N_{0\mathrm{dB}}} \tag{37}$$

for any PSF channel $i \in \{1, 2, \ldots, m\}$.

When all nodes operate with the same IpI $N_i = N_m = L_m + \delta N = const$, where δN is the maximum pulse-position offset in the encoding, then all PSF channels have the same spectral efficiency η and the same SIR margin, and they each support the same number of equal-payload nodes. With this, the ranges $d_0 \le d_{i-1} < d_i \le d_m = d_{\max}$ can be obtained from the condition

$$\int_{d_{i-1}}^{d_i} dr\, \phi(r) = \frac{1}{m} \quad \text{for any} \quad i \in \{1, 2, \ldots, m\}, \tag{38}$$

subject to the constraints

$$\langle \mathrm{SIR}\rangle_i^{-1} = \frac{\sum_{j=1}^m \left\langle \left(\frac{d_j}{r}\right)^\gamma \right\rangle_j}{\left\langle \left(\frac{d_i}{r}\right)^\gamma \right\rangle_i} - 1 \lesssim \frac{N_m}{\alpha\, N_{0\mathrm{dB}}}. \tag{39}$$

Then, given the value $D_m = 1 - \delta N/N_m$ for the nodes in the outermost partition, the pulse duty cycles D_i for the nodes in the i-th partition (PSF channel) can be obtained as

$$D_i = \left(\frac{d_i}{d_m}\right)^{\gamma} D_m. \tag{40}$$

Note that, in contrast to the case of constant-power nodes, the partition ranges obtained from (38) do not depend on the value of the path-loss exponent γ. In fact, (38) simply signifies the assignment of the PSF channels according to the ranges between the adjacent m-quantiles [22] of the path-loss values.

Next, let us make some quantitative comparisons between the equal-power and the equal-IpI approaches to M-ASPM network management. In particular, let us consider uniform areal coverage beyond range d_0 within a hexagonal cell with the circumradius $d_{\max} = d_m > d_0$. Note that, in order for an M-ASPM with constant-envelope pulses to operate in the spread-spectrum region, the equal-power node arrangement is subject to an additional constraint $N_1 > 4(M-1)/(1-D)$, where D is the pulse duty cycle. Thus, in the examples that follow, the values of d_0 are chosen to be sufficiently large, so both the equal-power and the equal-IpI approaches can be used and compared with each other.

A. IMPACT OF INTER-PSF INTERFERENCE ON NUMBER OF PSF CHANNELS

First, let us assess the impact of the inter-PSF interference on the total number of the PSF channels that can be used, under a given constraint on the deterioration in the BER, for a desired areal coverage.

1) NODES WITH EQUAL TRANSMIT POWER

Recall from our toy example in Section I that, for a given maximum range d_2, the total number of the PSF channels $(m_1 + m_2)$ for equal-power M-ASPM nodes depends on both the propagation conditions (the value of γ) and the shape of the node distribution (the values of d_1 and/or κ). Such strong dependence is also apparent in Fig. 12, for the uniform areal coverage beyond range d_0 within a hexagonal cell. For example, even for identical propagation conditions and thus identical maximum physical range d_m, the maximum number of the PSF channels that can be deployed under a given SIR constraint $N_m/(\alpha N_{0\mathrm{dB}})$ noticeably decreases with d_0, and thus with the increase in the coverage area. As the SIR for more remote nodes becomes larger with the relative increase in the received power of the nodes close to the gateway, the impact of inter-PSF interference on these remote nodes becomes more severe with the decrease in d_0 and/or the increase in γ.

2) EQUAL-IpI NODES

In contrast, as can be seen in Fig. 13, for the equal-IpI nodes the impact of the change in the areal distribution on the maximum number of the PSF channels is insignificant, and this number is also insensitive to variations in the value of γ.

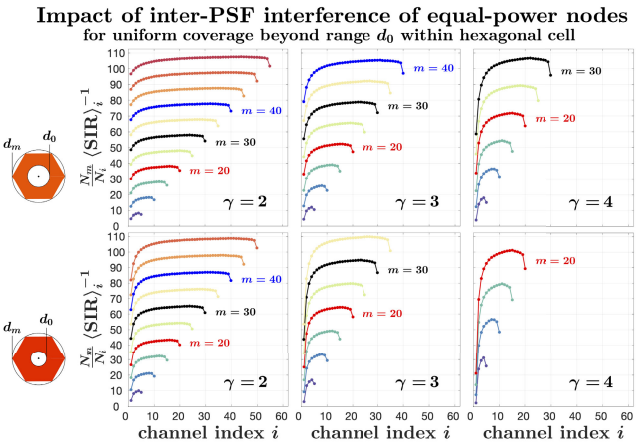

FIGURE 12. Impact of inter-PSF interference of equal-power nodes for uniform coverage beyond range d_0 within hexagonal cell with circumradius d_m for $m = 5, 10, 15, \ldots$ of PSF channels.

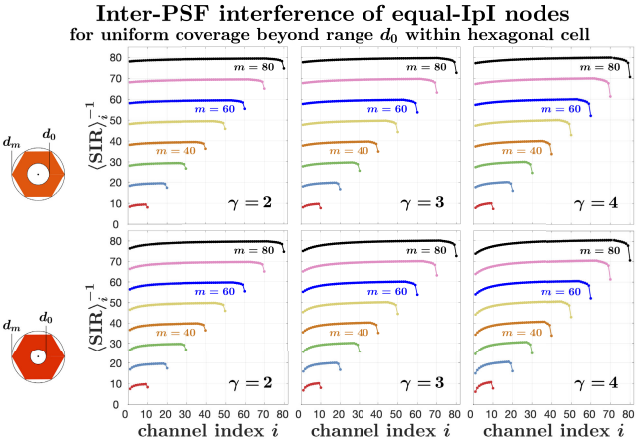

FIGURE 13. Impact of inter-PSF interference of equal-IpI nodes for uniform coverage beyond range d_0 within hexagonal cell with circumradius d_m for $m = 10, 20, 30, \ldots$ of PSF channels.

Further, note that the TBP of the convolution of any PSF $\hat{\zeta}$ with its complex conjugate is always larger than the TBP of $\hat{\zeta}$. In particular, for "flip" PSFs such that $\hat{\zeta}_2 = \zeta_1^*$, the TBP of $\hat{\zeta}_2 * \zeta_1 = \zeta_1^* * \zeta_1$ is about twice as large as the (already large) TBP of ζ_1. Thus a pair of "flip" PSFs can be used for two different PSF channels. Since these two channels will have the same duty cycle, they can be used in the same range interval. For example, the i-th pair of "flip" PSFs can be used for the range interval $[d_{i-1}, d_i]$.

For m such pairs, the inter-PSF constraint can be expressed as

$$\langle \mathrm{SIR}\rangle_i^{-1} = 2\,\frac{\sum_{j=1}^{m}\left\langle\left(\frac{d_j}{r}\right)^{\gamma}\right\rangle_j}{\left\langle\left(\frac{d_i}{r}\right)^{\gamma}\right\rangle_i} - 1 \lesssim \frac{N_m}{\alpha N_{0\mathrm{dB}}} \tag{41}$$

for any pair index $i \in \{1, 2, \ldots, m\}$. The SIR impact of the inter-PSF interference for equal-IpI "flip" PSF pairs is quantified in Fig. 14.

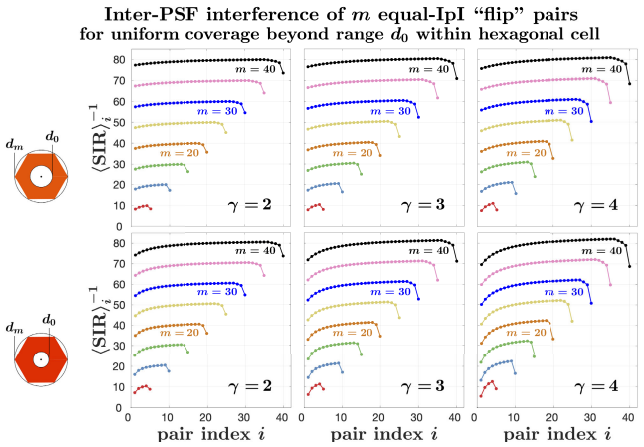

FIGURE 14. Impact of inter-PSF interference of equal-IpI "flip" PSF pairs for uniform coverage beyond range d_0 within hexagonal cell with circumradius d_m for $m = 5, 10, 15, \ldots$ of pairs.

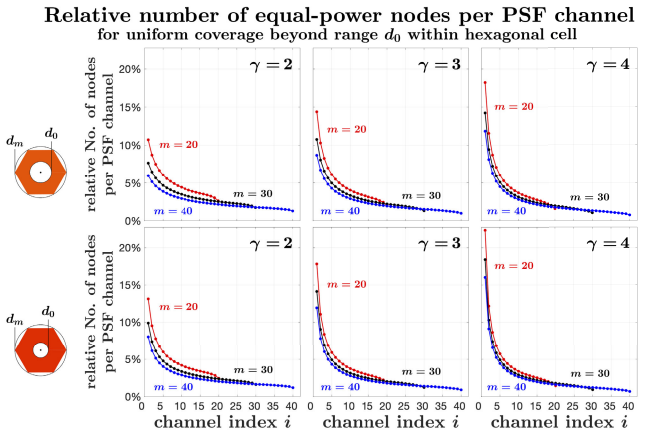

FIGURE 15. Relative number of equal-power nodes per PSF channel for uniform coverage beyond range d_0 within hexagonal cell.

As can be seen by comparing the interference impacts shown in Figs 13 and 14, by using "flip" PSFs we can reduce the number of the partition ranges and the pulse duty cycles by half, with only insignificant decrease in the total number of the PSF channels. As a bonus, using "flip" PSF pairs also automatically implements the suggestion (see Section III-B) to alternate "up-chirp" and "down-chirp" PSFs in order to lower the peakedness of the mutual interference, and thus its excessive impact on the BER, when reducing the pulse duty cycles for the closer-range nodes.

B. RELATIVE NUMBER OF NODES PER PSF CHANNEL

The total number of nodes for m PSF channels used for the areal coverage can be expressed as

$$C = \sum_{i=1}^{m} C_1(N_i) = C_1(N_m) \sum_{i=1}^{m} \frac{N_m}{N_i}, \tag{42}$$

where $C_1(N_i)$ is the number of nodes in a single PSF channel with the IpI N_i. Then the relative number of nodes in the i-th PSF channel is

$$\frac{C_1(N_i)}{C} = \frac{N_i^{-1}}{\sum_{j=1}^{m} N_j^{-1}} = \frac{1}{m} \frac{\overline{N}}{N_i}, \tag{43}$$

where $\overline{N}$ is the *harmonic mean* of $N_1, N_2, \ldots, N_m$.

1) NODES WITH EQUAL TRANSMIT POWER

For equal-power nodes,

$$\frac{C_1(N_i)}{C} = \frac{1}{m} \frac{\overline{N}}{N_i} = \frac{1}{m} \frac{\overline{d^\gamma}}{d_i^\gamma}, \tag{44}$$

where $\overline{d^\gamma}$ is the harmonic mean of $d_1^\gamma, d_2^\gamma, \ldots, d_m^\gamma$. Thus the nodes are distributed very unevenly among the PSF channels, and the relative number of nodes in a given channel varies strongly with a change in the areal distribution and/or in the propagation conditions. This is illustrated in Fig. 15.

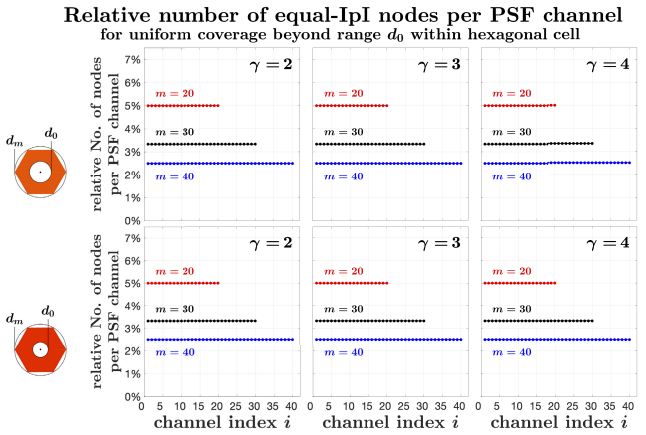

FIGURE 16. Relative number of equal-IpI nodes per PSF channel for uniform coverage beyond range d_0 within hexagonal cell.

2) EQUAL-IpI NODES

In contrast, as illustrated in Fig. 16, when all nodes use the same IpI $N_i = N_j = N_m$, then

$$\frac{C_1(N_i)}{C} = \frac{1}{m}, \tag{45}$$

and each PSF channel supports the same fraction of the total number of nodes for any areal distribution and/or the value of γ.

C. TOTAL NUMBER OF NODES WITHIN AREAL COVERAGE

The total number of nodes can be conveniently expressed in relation to the value of C_{lim} defined in (4), which is common to all IpIs and thus all ranges:

$$C_{\mathrm{lim}} = C_1(N_i) \frac{N_i}{\alpha N_{0\mathrm{dB}}} = C_1(N_m) \frac{N_m}{\alpha N_{0\mathrm{dB}}}. \tag{46}$$

Note that C_{lim} incorporates both the co-PSF constraint α and the SIR margin $N_i/N_{0\mathrm{dB}}$.

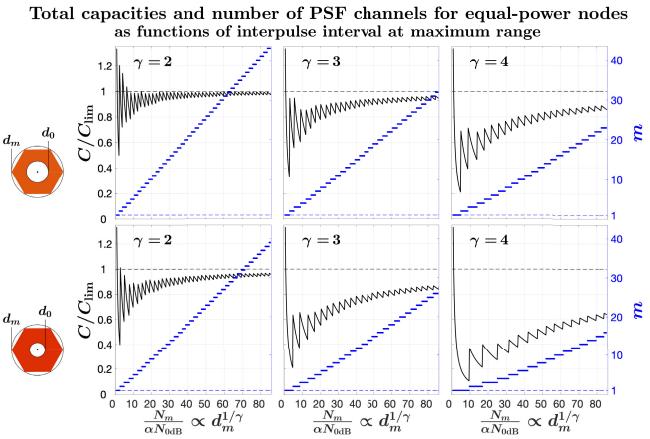

FIGURE 17. Total capacities and number of PSF channels for equal-power nodes, as functions of IpI at maximum range, for uniform coverage beyond range d_0 within hexagonal cell.

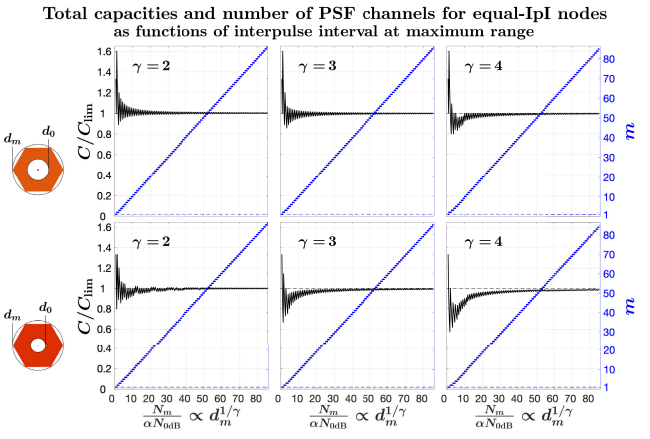

FIGURE 18. Total capacities and number of PSF channels for equal-IpI nodes as functions of IpI at maximum range for uniform coverage beyond range d_0 within hexagonal cell.

For nodes distributed within the range interval $[d_0, d_{\max}]$, from (42) we can obtain the limit

$$\lim_{d_0 \to d_{\max}} C = m\, C_1(N_m) = \left\lceil \frac{\Delta_{\mathrm{SIR}}(N_m)}{\alpha} \right\rceil C_1(N_m) = \left\lceil \frac{N_m}{\alpha\, N_{0\mathrm{dB}}} \right\rceil C_1(N_m) \approx C_{\lim} \quad \text{for } N_m \gg \alpha\, N_{0\mathrm{dB}}, \tag{47}$$

where $\lceil x \rceil$ is the ceiling function.

1) NODES WITH EQUAL TRANSMIT POWER

For the given radial distribution $\phi(r)$ of equal-power nodes, and the value of γ, the partition ranges d_i and the interpulse intervals N_i can be obtained from (36) for any m. For these values, the impact of the inter-PSF collisions can be assessed according to (37) (see, e.g., Fig. 13). Then the maximum achievable value of C can be calculated from (42) and (46) for the IpI values N_i obtained for the maximum value of m that satisfies the inter-PSF constraint (37). For example, in Fig. 17, the maximum number of the PSF channels that can be deployed, and the respective ratio $C/C_{\lim}$, are plotted as functions of the IpI N_m at the maximum range $d_m = d_{\max}$.

Note that, at long ranges, the total capacity (number of nodes) C of the equal-power arrangement approaches $C_{\lim}$ only when all interpulse intervals are sufficiently large, i.e.,

$$C \approx C_{\lim} \quad \text{for } N_1 = \left(\frac{d_1}{d_m}\right)^{\gamma} N_m \gg \alpha N_{0\mathrm{dB}}. \tag{48}$$

Thus, as can be seen in Fig. 17, the total number of nodes that can be deployed within the given maximum range $d_{\max}$ declines when more nodes are placed closer to the gateway (i.e., for smaller d_0), and this effect is more pronounced for large values of γ.

2) EQUAL-IpI NODES

In contrast, for equal-IpI nodes the condition (48) becomes simply

$$C \approx C_{\lim} \quad \text{for } N_m \gg \alpha N_{0\mathrm{dB}}. \tag{49}$$

For example, with the SIR margins for 16-ASPM and 64-ASPM depicted in Fig. 8, the total number of nodes approaches $C_{\lim}$, for any value of $\alpha < 1$, when the outermost range $d_{\max}$ exceeds approximately that of LoRa with SF = 9.

When all nodes use the same IpI N_m, then the partition ranges are the same for any γ, and can be easily obtained from (38). Then the maximum value of m can be obtained from (39), and the ratio $C/C_{\lim}$ can be calculated as $C/C_{\lim} = m\,\alpha\, N_{0\mathrm{dB}}/N_m$. As can be seen in Fig. 18, this ratio approaches unity for $m \gg 1$, for any value of γ and/or d_0.

D. ENERGY EFFICIENCY

The energy consumption $\mathcal{E}_i$ of a single node in the i-th PSF channel (i.e., the i-th partition) is proportional to the length of the PSF, that is, $\mathcal{E}_i \propto L_i = D_i N_i$. Then, in relation to the energy consumption of a node in the outermost partition, the average energy consumption per node can be expressed as

$$\frac{\mathcal{E}_{\mathrm{ave}}}{\mathcal{E}_m} = \frac{1}{\mathcal{E}_m} \frac{\sum_{i=1}^{m} C_1(N_i)\,\mathcal{E}_i}{\sum_{i=1}^{m} C_1(N_i)} = \frac{\overline{N}}{N_m} \frac{\langle D \rangle}{D_m} \le 1, \tag{50}$$

where $\overline{N}$ is the harmonic mean of $N_1, N_2, \ldots, N_m$, and $\langle D \rangle$ is the *arithmetic mean* of $D_1, D_2, \ldots, D_m$. When all nodes operate with the same duty cycle, (50) becomes

$$\frac{\mathcal{E}_{\mathrm{ave}}}{\mathcal{E}_m} = \frac{\overline{N}}{N_m} = \frac{\overline{d^{\gamma}}}{d_m^{\gamma}} \le 1, \tag{51}$$

where $\overline{d^{\gamma}}$ is the harmonic mean of $d_1^{\gamma}, d_2^{\gamma}, \ldots, d_m^{\gamma}$. In contrast, when all nodes operate with the same IpI, (50) becomes

$$\frac{\mathcal{E}_{\mathrm{ave}}}{\mathcal{E}_m} = \frac{\langle D \rangle}{D_m} = \frac{\langle d^{\gamma} \rangle}{d_m^{\gamma}} \le 1, \tag{52}$$

where $\langle d^{\gamma} \rangle$ is the arithmetic mean of $d_1^{\gamma}, d_2^{\gamma}, \ldots, d_m^{\gamma}$.

On the one hand, as compared to the harmonic mean, the arithmetic mean is biased toward larger values. On the other hand, for a given radial node density $\phi(r)$ the partition ranges d_i for the equal-IpI partitioning are biased toward smaller values than those for the equal-power partitioning

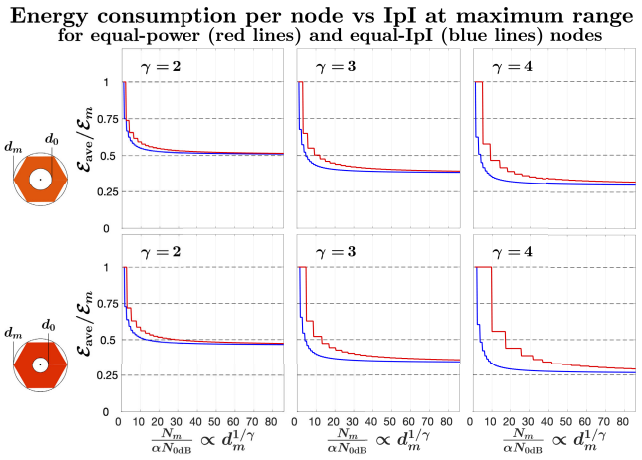

FIGURE 19. Energy consumption per node vs IpI at maximum range for equal-power (red lines) and equal-IpI (blue lines) nodes, for uniform coverage beyond range d_0 within hexagonal cell.

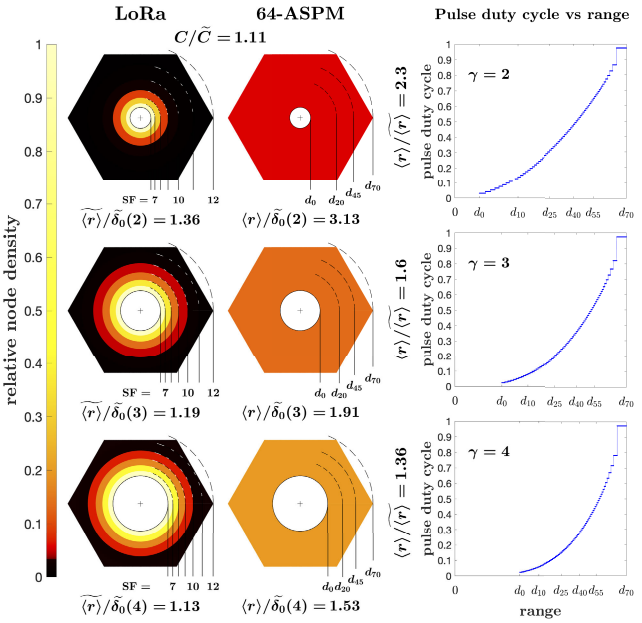

FIGURE 20. Example of areal coverage beyond range d_0, equal to range of LoRa with SF = 6, within hexagonal cell with circumradius equal to range of LoRa with SF = 12. (Actual physical ranges are different for different path-loss exponents γ.)

(compare, e.g., (36) and (38)). As the net result, the average energy consumption per node in the equal-IpI case remains below that for the equal-power nodes. This is illustrated in Fig. 19. Note that, just like for the total number of nodes (compare, e.g., Figs. 17 and 18), the difference in the energy efficiency between the two arrangements becomes more pronounced when more nodes are placed closer to the gateway (i.e., for smaller d_0), and for larger values of γ.

V. WIDE AREAL COVERAGE WITH M-ASPM AS COMPARED TO LoRa

Let us now illustrate the main contrast between LoRa and equal-IpI M-ASPM when both are used for wide areal coverage.

In LoRa, the extension of the range is accomplished by incrementing the SF, which represents the number of bits per LoRa waveform, thus also slightly increasing the energy-per-bit efficiency. However, this increase is insignificant in comparison with the reduction in the spectral efficiency $\widetilde{\eta}$, and any decrease in $\widetilde{\eta}$ is not accompanied by the respective increment in the number of available SF channels operating at this spectral efficiency. Say, if we can ignore the impact of inter-SF collisions, then in a single-gateway LoRa network with SF $\in \{7, 8, \ldots, 12\}$ all six SF channels can be used in the range below that for SF $= 7$. At the same time, the range between SF $= 10$ and SF $= 11$ can be served by only two channels, and only one SF channel (with SF $= 12$) can be employed in the range above SF $= 11$. At the same time, a single increment in the SF approximately doubles the ToA of a given payload, proportionally reducing the number of nodes (as well as their energy efficiency). As a result, the effective range of LoRa (defined, e.g., as the mean distance of the transmitters from the receiver, weighted by their payloads) is heavily biased toward the range for the smallest SF. For example, in a single-gateway LoRa network with SF $\in \{7, 8, \ldots, 12\}$, operating at full capacity, about 45% of the nodes are confined to the range below that for SF $= 7$, and more than 70% of the nodes are within the range for SF $= 8$. Thus the effective range of such LoRa network, expressed as the average distance of the nodes from the gateway, remains below the range for SF $= 8$.

In contrast, M-ASPM allows capacity-preserving range extension for numerous areal distributions of the uplink nodes, including those with the effective range approaching the maximum range. For example, as can be seen in the upper panel of Fig. 1, the value of $C_{\rm lim}$ for 64-ASPM exceeds the total number of nodes in LoRa with SF $\in \{7, 8, \ldots, 12\}$. Thus, within a given maximum range, a 64-ASPM gateway can serve slightly more uplink nodes than LoRa, and at a significantly larger effective range. This is illustrated in Fig. 20 for the areal coverage beyond the range d_0, equal to the range of LoRa with SF $= 6$, within a hexagonal cell with the circumradius equal to the range of LoRa with SF $= 12$. For this maximum range, $\alpha = 1/2$, and the SIR margin $\Delta_{\rm SIR}(d_{\max})$ for BER$'$/BER $= 10^{-3}/10^{-4}$, 70 PSF channels can be used for 64-ASPM, i.e., $d_{\max} = d_{70}$. Note that for the area within d_0 both LoRa and a single-channel 64-ASPM can provide identical coverage (see Fig. 5), hence we are interested only in the extension beyond this rage.

For LoRa, in each portion of the coverage within an annulus formed by the ranges for two adjacent SFs, we use the same (uniform) node density. With this constraint, the LoRa effective range is maximized when all nodes within such a portion of the coverage operate with the same SF, equal to the largest of the two adjacent SFs. For 64-ASPM, the node density is uniform for the whole coverage area. For such uniform 64-ASPM node density, in Fig. 20 the effective ranges $\widetilde{\langle r\rangle}$ and $\langle r\rangle$ for LoRa and 64-ASPM are presented

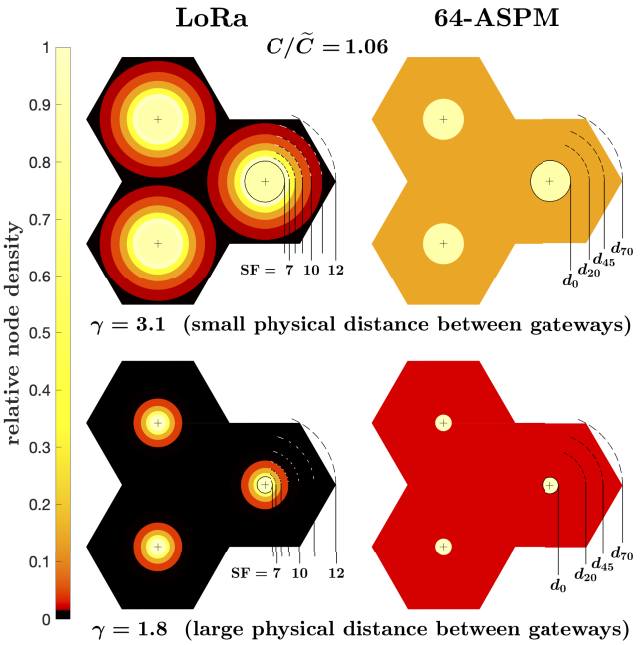

FIGURE 21. Contrast between LoRa and M-ASPM when multiple gateways are used for wide areal coverage. Range d_0 is equal to range of LoRa with SF = 6, and within this range LoRa and single-channel 64-ASPM provide identical node densities.

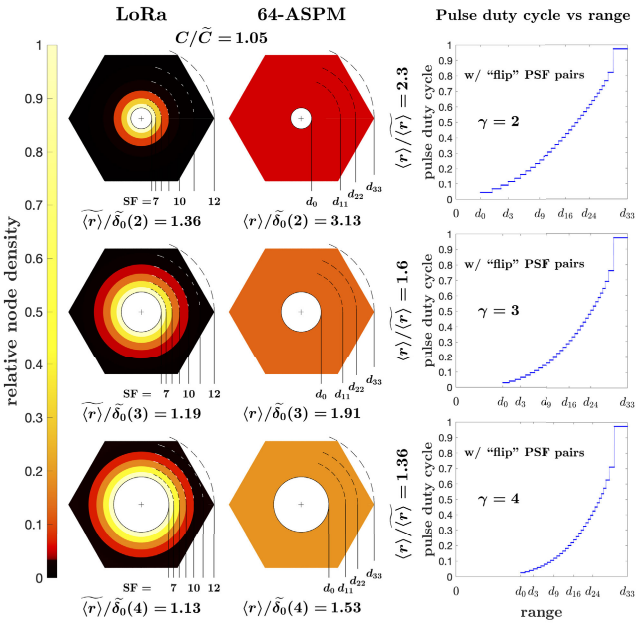

FIGURE 22. Using pairs of "flip" PSFs results in only small decrease in M-ASPM capacity, while reducing number of pulse duty cycles and partitions by more than half.

in relation to $\widetilde{\delta}_0(\gamma)$ and to each other. One can see that the effective range of 64-ASPM is noticeably larger than that of LoRa.

Note that a constant value for the 64-ASPM node density over the whole area is chosen simply as a desired "benchmark" feature for the areal coverage, and not for maximizing its effective range. Needless to say, the node distribution in 64-ASPM can vary widely, based on the desired placement of the nodes, without affecting their total number. For example, the 64-ASPM's node density can match that of LoRa, so that $\Phi(\varphi, r) = \widetilde{\Phi}(\varphi, r)$, or *complement* that of LoRa to achieve the desired density $\Phi_0(\varphi, r)$, so that

$$\Phi(\varphi, r) = \left(1 + \frac{\widetilde{\mathcal{C}}}{\mathcal{C}}\right) \Phi_0(\varphi, r) - \frac{\widetilde{\mathcal{C}}}{\mathcal{C}}\, \widetilde{\Phi}(\varphi, r), \qquad (53)$$

where $\widetilde{\mathcal{C}}$ and $\mathcal{C}$ are the total numbers of nodes for LoRa and 64-ASPM, respectively. However, as relatively more nodes are placed closer to the maximum range, the extension of the effective range within a given maximum range comes at some unavoidable penalty on the energy efficiency. This is signified by (52), and can be seen by comparing the upper and the lower panels in Fig, 19.

As was mentioned in Section III, we use the simple power-law path loss model for illustration of the main scaling properties of M-ASPM, and for its comparison with LoRa. In fact, empirical data for the LoRa long-distance path loss show that, when the value of the path-loss exponent is chosen according to the specific environment and to the maximum physical range, this simple model may be adequate for the overall assessment of the network coverage [14], [15], [16], [17]. For example, for the city of Bonn (Germany), with a flat topography and a typical urban environment with tall and medium-sized buildings, the authors report in [17] the values of $\gamma \gtrsim 3$ for the ranges approximately below 2 km, and $\gamma \lesssim 2$ for the ranges above 6 km, with the value of the path-loss exponent eventually decaying to $\gamma \approx 1.6$ at longer rages. For such a case, Fig. 21 illustrates the contrast between LoRa and M-ASPM when multiple gateways (e.g., operating in different frequency bands) are used for wide areal coverage. The range d_0 is equal to the range of LoRa with SF = 6, and within this range LoRa and a single-channel 64-ASPM provide identical node densities. The difference in the maximum physical ranges (i.e., the range for SF = 12) can be due, for example, to differences in the bandwidth and/or in the maximum transmit power.

Further, as discussed in Section IV-A2, a pair of "flip" PSFs can be used for two different PSF channels sharing the same duty cycle. Using "flip" PSFs leads to only insignificant decrease in the total number of the PSF channels, and thus the total number of nodes, while significantly reducing the number of the partition ranges and the pulse duty cycles. For example, as can be seen in Fig. 22, using "flip" PSF pairs for the coverage shown in Fig. 20 reduces the number of the PSF channels in 64-ASPM from 70 to 66, resulting in less than 6% decline in the total number of nodes. At the same time, the number of the partition ranges and the pulse duty cycles is reduced by more than half, from 70 down to 33. Thus using "flip" PSF pairs can noticeably simplify practical deployment and management of M-ASPM networks.

VI. DISCUSSION

Even in an ideal world of well-known path attenuation for each node, managing an M-ASPM network with equal-power

nodes can be a complicated task. Indeed, a change in the path loss of some nodes impacts their SNR. Then we would need to adjust these nodes' IpIs to maintain the target BER. Clearly, this changes the SIR margins of these nodes, and thus their tolerance to the inter-PSF interference. However, such a modification in the IpI also changes the ToA, and thus the channel utilization for these nodes. This, in turn, affects the SIR values of the mutual interference for all other nodes. As the result, reconfiguring the network in a manner that maximizes its capacity, that is, so that all PSF channels are fully utilized, requires solving a system of nonlinear equations and inequalities representing these interdependencies. Then we would need to make the respective modifications to the data rates of individual nodes (i.e., in their IpIs), the total number of the PSF channels, and the number of nodes per channel. These solutions, however, may be highly sensitive to the accuracy of the path-loss data. In addition, for a wide range of path losses, excessively strong interference from the nodes with a small path attenuation can noticeably lower the total network capacity and the average energy efficiency of the nodes.

In contrast, if we are able to adjust the transmit powers of the nodes proportionally to the path-loss changes, all other parameters of these and all other nodes in the network remain unchanged. If we can control the transmit power of nodes without sacrificing the transmission efficiency, then the energy efficiency of the network does not deteriorate. In this paper, we outline a practical approach to implementing such an energy-efficient M-ASPM power control, that can be used for scaling LPWANs with realistic desired and/or actual areal distributions of the uplink nodes under different propagation conditions.

In our presentation, one of the main simplifying assumptions was that the path loss is a monotonically increasing, and thus invertible, function of the range. Then the node density function $\Phi(\varphi, r)$ allows us to estimate the path-loss dependent parameters of the nodes according to their locations. Therefore, $\Phi(\varphi, r)$ becomes a useful analytical tool for a meaningful comparison between the equal-power and the equal-IpI M-ASPM arrangements, and between LoRa and M-ASPM. In many practical environments, however, the path loss may be neither monotonic nor even single-valued function of the range.

Nevertheless, let us assume that we can reasonably accurately obtain the values of the path loss, specific to the gateway, for each node. This can be done, for example, in a manner described in Section III. Further, let us use the equal-IpI M-ASPM approach to network management. Then the capacity of a single-gateway network can be maximized under the guideline of a basic procedure outlined below.

First, for a sufficiently large N_m, the number of the PSF channels can be calculated as $m = \lfloor N_m/(\alpha N_{0\mathrm{dB}})\rfloor \gg 1$. Next, we can obtain the values $\mathcal{L}_i$, $i \in \{1, 2, \ldots, m\}$, for m-quantiles [22] of the nodes' path losses. Provided that $\mathcal{L}_i > \mathcal{L}_{i-1}$, the nodes with the path loss between the $(i-1)$-th and the i-th m-quantiles (i.e., in the interval $]\mathcal{L}_{i-1}, \mathcal{L}_i]$) are assigned to the i-th PSF channel, and their duty cycles are set to $D_i = (\mathcal{L}_i/\mathcal{L}_m)\, D_m$. With this, if the total number of nodes is much larger than the number of the PSF channels, all channels will contain approximately equal numbers of nodes and will have effectively the same utilization. Subsequently, the payloads of the nodes can be maximized according to the co-PSF constraint α. In addition to its conceptual simplicity, this equal-IpI approach is also more robust to changes in the propagation conditions, and to imprecisions in the path-loss data.

Among appealing features of M-ASSPM is its extensive versatility in trading multiple PHY parameters to reconcile often conflicting LPWAN technical concerns. In this paper, a major such concern was the transmission efficiency. Therefore, we imposed the equal-amplitude constraint on the M-ASPM pulses. Then the transmit power becomes proportional to the pulse duty cycle, and this can be used for energy-efficient M-ASPM power control. However, other technical requirements can be equally or even more important than the energy efficiency, thus requiring various adjustments to the M-ASPM parameters, and/or additional constraints on these parameters.

For instance, it may be desired that all M-ASPM links within the coverage area are insensitive to the nodes' motion with the speeds below some value Δv. If we use the value $3c/(4\pi^{1/2}\Delta v f_c)$ for the Doppler coherence time [23], where f_c is the carrier frequency and c is the speed of light, then the PSF length L would be constrained by the condition

$$L = DN_p \lesssim 0.423\, \frac{F_s}{f_c}\, \frac{c}{\Delta v}. \tag{54}$$

For example, for the maximum 64-ASPM range corresponding to LoRa with SF $= 12$, the carrier frequency $f_c = 915$ MHz, 500 kHz bandwidth, and $\Delta v = 40$ m/s (90 mi/h), the pulse duty cycle would be restricted to below about 56%.

Or, for the pulse-position encoding, performance of noncoherent M-ASPM in multipath propagation can be improved by increasing the minimum time interval between the pulse positions corresponding to different symbols, so that this interval becomes sufficiently large with respect to the delay spread. This minimum time interval can be expressed as $\lfloor \delta N/(M-1)\rfloor/F_s$, where the maximum pulse-position offset δN in the encoding is subject to the inequalities

$$4(M-1) \le \delta N \le \lfloor (1-D)\, N_p \rfloor. \tag{55}$$

Thus, for a given IpI, increasing M-ASPM's resistance to delay spreads may require reduction in the pulse duty cycle. This may need to be taken into account when choosing the maximum pulse duty cycle D_m in the equal-IpI M-ASPM. For example, for 500 kHz bandwidth and the maximum 64-ASPM range corresponding to LoRa with SF $= 12$, to exceed 25 μs minimum time interval between the pulse positions (corresponding to the distance of 7.5 km) would require that $D_m \lesssim 75\%$.

VII. CONCLUSION

By providing long range wireless access to the Internet of Things (IoT), various LPWAN technologies have been one of the main drivers of the IoT expansion. In this paper, our main focus was to outline a practical approach to implementing an energy-efficient M-ASPM power control, that can be used for scaling LPWANs with realistic desired and/or actual areal distributions of the uplink nodes under diverse propagation conditions. As we demonstrate, M-ASPM is particularly well suited for development of energy-efficient and highly practically scalable LPWANs, adding to the flexibility in addressing a broader range of IoT applications, both static and mobile.

APPENDIX A
ACRONYMS

ACF: autocorrelation function; A/D: Analog-to-Digital; ASPM: Aggregate Spread Pulse Modulation; AWGN: Additive White Gaussian Noise; BER: Bit Error Rate; CDMA: Code Division Multiple Access; D/A: Digital-to-Analog; IoT: Internet of Things; IpI: Interpulse Intrval; LoRa: Long Range (modulation technique for LPWANs based on chirp spread spectrum); LPWAN: Low-Power Wide Area Network; M-ASPM: M-ary ASPM; PA: Power Amplifier; PAPR: Peak-to-Average Power Ratio; PHY: physical layer; PSD: Power Spectral Density; PSF: Pulse Shaping Filter; RC: Raised-Cosine; SF: Spreading Factor (for LoRa); SIR: Signal-to-Interference Ratio; SINR: Signal-to-Interference-plus-Noise Ratio; SNR: Signal-to-Noise Ratio; TBP: Time-Bandwidth Product; ToA: Time-on-Air.

APPENDIX B
COMMENTS ON NOTATIONS

Whenever a particular notation is introduced in the paper, it is immediately defined. Some notations are used only once. The notations that are used consistently (and more that once) throughout the paper include:

α	co-PSF collisions constraint (channel utilization)
B	bandwidth
β	roll-off factor of RC pulse
C	network capacity or number of end nodes (with or without subscripts)
d	range or distance between transmitter and receiver (with or without subscripts)
D	pulse duty cycle (with or without subscripts)
$\widetilde{\delta}_0(\gamma)$	range of LoRa with SF = 7
Δ_{SIR}	SIR margin
E_{b}	energy per bit
$\mathcal{E}_i$	energy consumption of node in i-th PSF channel
η	spectral efficiency (with or without subscripts)
f_{b}	bit rate
f_{p}	pulse rate
F_{s}	sample rate
φ	angular coordinate (in density function; with or without subscripts)
$\phi(r)$	radial node density
$\Phi(\varphi, r)$	node density function expressed in polar coordinates centered at gateway
γ	path-loss exponent (in power-law path loss)
Γ	SNR
Γ'	SINR
k	sample index (in digital signal representations)
L	PSF length (with or without subscripts)
M	number of states in M-ary encoding
N	average interpulse interval (with or without subscripts)
$N_{0\mathrm{dB}}$	average interpulse interval for 0 dB SIR margin
$\mathcal{N}_0$	one-sided noise PSD
$\mathcal{N}_{\mathrm{s}}$	oversampling factor
P_{b}	bit error probability
r	distance from receiver/gateway (radial coordinate in density function)

Some notations may have different contextual meaning in different parts of the paper. This change in meaning normally affects the letters commonly representing integer numbers (e.g., "i" and "j"), such as subscripts and/or summation indices. For example, the letter "j" can be used as the (integer) number indicating a particular pulse in the designed pulse sequence $\hat{x}[k]$ (e.g., k_j is the sample index of the j-th pulse, and m_j is its "state"). However, j may also relate to the j-th transmitter, or j-th range value, or j-th pair of "flip" PSFs. Whenever such change occurs, the respective clarification is provided.

In the mathematical notations we reserve the letters "ζ," "g," and "h" for pulse shaping filters, with g and h being the real and the imaginary parts, respectively, of ζ. For example, we denote the finite impulse response of a PSF applied to a designed pulse train as $\hat{\zeta}[k]$, where k is the sample index. As the focus in this paper is on the single-sideband M-ASPM, the PSF components g and h are related to each other through the Hilbert transform, e.g., $h(t) = \pm H(g)(t)$ (in analog domain) or $h[k] = \pm H\{g[k]\}$ (in digital representation).

To distinguish between the respective quantities for LoRa and M-ASPM, those for LoRa are marked by overhead tildes.

Further, we find it convenient to use the "hat" operator for $\hat{\zeta}[k]$, $\hat{g}[k]$, and $\hat{h}[k]$ to distinguish them from their respective matched filters $\zeta[k] = \hat{\zeta}^*[-k]$, $g[k] = \hat{g}[-k]$, and $h[k] = \hat{h}[-k]$. We also use the hat symbol in Section II to denote the designed pulse train $\hat{x}[k]$, as opposed to the shaped trains obtained by applying PSFs to the designed pulse sequence.

REFERENCES

[1] A. V. Nikitin and R. L. Davidchack, "M-ary aggregate spread pulse modulation in LPWANs for IoT applications," in *Proc. IEEE Global Commun. Conf. (GLOBECOM)*, Madrid, Spain, Dec. 2021, pp. 1–7.

[2] A. V. Nikitin and R. L. Davidchack, "M-ary aggregate spread pulse modulation for robust and scalable low-power wireless networks," *IEEE Access*, vol. 10, pp. 96652–96671, 2022.

[3] N. Abramson, "The ALOHA system: Another alternative for computer communications," in *Proc. Int. Workshop Manag. Requirements Knowl. (AFIPS)*, Houston, TX, USA, Nov. 1970, pp. 281–285, doi: 10.1145/1478462.1478502.

[4] A. Kumar, D. Manjunath, and J. Kuri, *Wireless Networking*. San Mateo, CA, USA: Morgan Kaufmann, 2008.

[5] L. Vangelista, "Frequency shift chirp modulation: The LoRa modulation," *IEEE Signal Process. Lett.*, vol. 24, no. 12, pp. 1818–1821, Dec. 2017.
[6] G. Baruffa, L. Rugini, L. Germani, and F. Frescura, "Error probability performance of chirp modulation in uncoded and coded Lora systems," *Digit. Signal Process.*, vol. 106, Nov. 2020, Art. no. 102828.
[7] A. V. Nikitin, "Communications method and apparatus," U.S. Patent 0 314 201 A1, Oct. 7, 2021.
[8] D. E. Knuth, "Two notes on notation," *Amer. Math. Monthly*, vol. 99, no. 5, pp. 403–422, May 1992, doi: 10.1080/00029890.1992.11995869.
[9] R. N. Bracewell, *The Fourier Transform and Its Applications*, 3rd ed. New York, NY, USA: McGraw-Hill, 2000.
[10] G. Todoran, R. Holonec, and C. Iakab, "Discrete Hilbert transform. Numeric algorithms," *Acta Electroteh.*, vol. 49, no. 4, pp. 485–490, 2008.
[11] D. Gabor, "Theory of communication," *J. Inst. Elect. Eng.*, vol. 93, no. 3, pp. 429–457, 1946, doi: 10.1049/ji-3-2.1946.0074.
[12] M. Vetterli and J. Kovačevic, *Wavelets and Subband Coding*. Upper Saddle River, NJ, USA: Prentice-Hall, 1995.
[13] J. G. Proakis and D. G. Manolakis, *Digital Signal Processing: Principles, Algorithms, and Applications*, 4th ed. Upper Saddle River, NJ, USA: Prentice-Hall, 2006.
[14] J. Petajajarvi, K. Mikhaylov, A. Roivainen, T. Hanninen, and M. Pettissalo, "On the coverage of LPWANs: Range evaluation and channel attenuation model for LoRa technology," in *Proc. 14th Int. Conf. ITS Telecommun. (ITST)*, Dec. 2015, pp. 55–59.
[15] P. Jorke, S. Bocker, F. Liedmann, and C. Wietfeld, "Urban channel models for smart city IoT-networks based on empirical measurements of LoRa-links at 433 and 868 MHz," in *Proc. IEEE 28th Annu. Int. Symp. Pers., Indoor, Mobile Radio Commun. (PIMRC)*, Oct. 2017, pp. 1–6.
[16] R. Ramesh, M. Arunachalam, H. Atluri, S. Anand, P. Arumugam, and B. Amrutur, "LoRaWAN for Smart Cities: Experimental study in a campus deployment," in *LPWAN Technologies for IoT and M2M Applications*, B. S. Chaudhari and M. Zennaro, Eds. New York, NY, USA: Academic, 2020, pp. 327–345.
[17] M. Rademacher, H. Linka, T. Horstmann, and M. Henze, "Path loss in urban LoRa networks: A large-scale measurement study," in *Proc. IEEE 94th Veh. Technol. Conf. (VTC-Fall)*, Sep. 2021, pp. 1–6.
[18] D. Torrieri, *Principles of Spread-Spectrum Communication Systems*, 4th ed. Boston, MA, USA: Springer, 2018.
[19] A. V. Nikitin and R. L. Davidchack, "Hidden outlier noise and its mitigation," *IEEE Access*, vol. 7, pp. 87873–87886, 2019.
[20] A. V. Nikitin and R. L. Davidchack, "Pulsed waveforms and intermittently nonlinear filtering in synthesis of low-SNR and covert communications," *IEEE Access*, vol. 8, pp. 173250–173266, 2020.
[21] P. A. M. Dirac, *The Principles of Quantum Mechanics*, 4th ed. London, U.K.: Oxford Univ. Press, 1958.
[22] H. A. David and H. N. Nagaraja, *Order Statistics* (Wiley Series in Probability and Statistics), 3rd ed. Hoboken, NJ, USA: Wiley, 2004.
[23] T. S. Rappaport, *Wireless Communications: Principles and Practice* (Prentice-Hall Communications Engineering and Emerging Technologies Series), 2nd ed. Upper Saddle River, NJ, USA: Prentice-Hall, 2002.

ALEXEI V. NIKITIN is a co-founder and Chief Science Officer of the Kansas-based Nonlinear LLC. He initiated his undergraduate and graduate studies in physics, chemistry, and engineering in the former USSR at Novosibirsk State University in Novosibirsk and Karpov Institute of Physical Chemistry in Moscow. After receiving a Ph.D. degree in physics from the University of Kansas in 1998, Dr. Nikitin led Research and Development work focused on methods and tools in nonlinear signal processing at several startup companies, some of which were subsequently acquired, specializing in applications in communications, power electronics, navigation, geophysical sciences, neurology, and biometrics. He is named as a first or sole inventor on over 30 issued US patents.

RUSLAN L. DAVIDCHACK is Professor of Mathematical Modeling and Computation at the School of Computing and Mathematical Sciences, University of Leicester, U.K. His research interests are in developing computational methods and tools for applications in molecular simulations, nonlinear dynamics and signal processing.

He received his undergraduate degree in theoretical condensed matter physics from Lviv University, Ukraine, and the Ph.D. degree in computational statistical physics from the University of Kansas. He has developed several unique computational approaches and made significant contributions to a variety of fields in computational chemistry, signal processing, mathematics, statistical physics, and biochemistry. He has an extensive track record of interdisciplinary collaborations which span academic institutions (e.g. Georgia Tech; UC Berkeley; Oxford, UK; EPFL, Switzerland; NTNU, Norway; KTH, Sweden), national laboratories in the USA (e.g. AFRL, Oak Ridge, Sandia), and UK (Daresbury, Institute of Pharmaceutical Innovation), and industrial partners (Tata Steel, Rolls-Royce, GlaxoSmithKline, Procter & Gamble). He has given invited talks at many international conferences in the USA, U.K., France, Germany, South Korea, China, and Ukraine.

Dr. Davidchack is a co-inventor of the AVATAR methodology, which provided the initial foundation for the technology of intermittently nonlinear outlier noise mitigation.